NASA Contractor Report 3563

Investigation of Spray Characteristics for Flashing Injection of Fuels Containing Dissolved Air and Superheated Fuels

A. S. P. Solomon, L-D. Chen,
and G. M. Faeth

GRANT NSG-3306
JUNE 1982

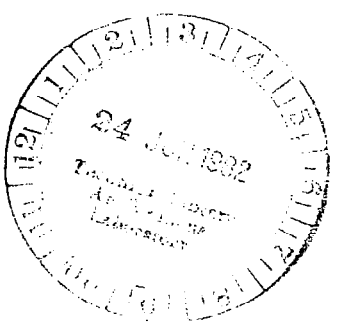

NASA

NASA Contractor Report 3563

Investigation of Spray Characteristics for Flashing Injection of Fuels Containing Dissolved Air and Superheated Fuels

A. S. P. Solomon, L-D. Chen,
and G. M. Faeth
The Pennsylvania State University
University Park, Pennsylvania

Prepared for
Lewis Research Center
under Grant NSG-3306

National Aeronautics
and Space Administration

Scientific and Technical
Information Office

1982

Investigation of Spray Characteristics for Flashing Injection of Fuels Containing Dissolved Air and Superheated Fuels

SUMMARY

This report discusses activities under NASA Grant No. NSG 3306 for the period September 1, 1980 to August 31, 1981. The objective of the investigation was to determine the amount of air that could be dissolved in Jet A fuel at high pressures and to study the thermodynamic, atomization and combustion properties of Jet A fuels containing dissolved air. Air solubilities and thermodynamic properties of Jet A/air mixtures were considered in the initial phase of this investigation, reported in Ref. 1. Work during this report period concentrated on injection and combustion properties of Jet A fuels containing dissolved air. This information can be applied to supercritical or flashing injection concepts.

Supercritical or flashing injection involves dissolving air into a fuel prior to injection. Upon injection the air comes out of solution (flashing) forming a vapor phase within the liquid. A similar effect can be obtained by preheating the fuel so that a portion of the fuel flashes when its pressure is reduced. Flashing is known to improve atomization properties and the presence of air in the primary zone of a spray flame is known to reduce the formation of pollutants. Therefore, the approach has been proposed as a means of improving the combustion characteristics of sprays.

The objectives of the present investigation can be summarized as follows:

1. Investigate the atomization properties of flashing liquids, including fuel/dissolved gas systems. Determine and correlate the effect of inlet properties and injector geometry on mass flow rates, Sauter mean diameters (SMD) and spray angles. The injector configuration is limited to straight-hole orifices with no swirl.
2. Examine the combustion properties of flashing injection in an open burner flame, particularly considering effects of dissolved gas levels and injector operating conditions on flame shape.

The results of the investigation can be summarized as follows:

1. The beneficial effects of flashing injection for dissolved gas systems could only be obtained by installing an expansion chamber in the injector passage (this involves a flow restriction followed by a small chamber to allow the dissolved gas to flash and equilibrate prior to entering the injector orifice). In contrast, an expansion chamber was not needed to obtain significant atomization improvements for flashing superheated pure liquids. This effect is due to the relatively slow bubble growth rates for dissolved gas systems in comparison to flashing pure liquids, which require additional residence time to equilibrate.

2. For given upstream conditions, there is an optimum expansion chamber pressure where the spray angle is maximized and the Sauter mean diameter (SMD) is minimized. This condition yields the shortest flame length and probably the least soot, similar to conventional behavior when atomization is improved for a combusting spray.

3. The flow properties of flashing injectors could be estimated using either a locally homogeneous or separated two-phase flow model, upon specification of a single empirical flow coefficient. Both these models indicated that increased spray angles were associated with choked injector flow, followed by significant external expansion of the two-phase flow.

4. SMD varied with axial position in the spray due to secondary breakup, drop collisions and turbulent dispersion of drops. For a fixed position in the spray, however, it was possible to correlate drop sizes for neat liquid injection and for flashing injection of liquids containing dissolved gases using conventional correlations for pressure atomized and airblast injectors.

5. It was found that the expansion chamber acts very similar to the mixing chamber of an airblast injector. Therefore, many of the effects observed during this study of flashing injection with dissolved gases could be obtained in a more conventional manner using airblast injector principles. The advantage of the airblast injector is that air concentrations are not limited by the solubility of the fuel, allowing more air to be mixed with the fuel and avoiding the need to compress the air to high pressures in order to dissolve appreciable quantities of air in the fuel.

6. The flashing injector concept is favored when high pressure gas is readily available, e.g., gas pressurized fuel feed systems. In this case, improved atomization can be obtained by allowing the pressurizing gas to dissolve in the liquid and installing an expansion chamber in the injector passage. The widespread use of household spray cans is a notable example of this approach. Similar behavior could be obtained by preheating a fuel under pressure so that volatile fractions can be released in an expansion chamber. With either method, the present results indicate that significant modifications of SMD and spray angles can be obtained with relatively low concentrations of flashed gases or vapors (less than 3% by mass).

TABLE OF CONTENTS

NOMENCLATURE

Symbol	Description
A	cross-sectional area
B	empirical parameter, Eq. (21)
B'	empirical parameter, Eq. (23)
C_f	flow coefficient
C_p	specific heat at constant pressure
d_i	mean drop diameter of group i
d_p	injector orifice diameter
D	expansion chamber diameter
E	empirical parameter, Eq. (22)
f	Fanning friction factor
F	fugacity
g	acceleration of gravity
G	mass velocity
k	specific heat ratio
$\dot{m}$	mass flow rate
N	number of drop size groups
p	pressure
r	radial distance
Re	Reynolds number
SMD	Sauter mean diameter
T	flow parameter, Eq. (6); temperature
u	axial velocity
w_i	weight fraction of drops in group i

Symbol	Description
x	mass quality
z	axial distance
α	void fraction
η_n	nozzle efficiency, Eq. (25)
θ	tube inclination from horizontal
μ	absolute viscosity
ρ	density
σ	surface tension

Subscripts

c	injector exit condition
cs	choked injector exit condition
e	expansion chamber condition
f	liquid
g	vapor or gas
u	condition upstream of injector
∞	ambient condition of injector

1. INTRODUCTION

Many practical propulsion and power systems, e.g., aircraft propulsion, industrial gas turbines, diesel engines, etc., involve combustion of fuel sprays. Liquid fuels that will be available in the future, coal derived liquids, shale oil, etc., present new difficulties with regard to their atomization and combustion properties. Supercritical injection [2],* and the related process of flashing injection [3], are receiving attention as a means of improving atomization and combustion properties of fuels in order to reduce the impact of these problems. The objective of this investigation is to develop a better understanding of the thermodynamic, flow and combustion properties of the supercritical or flashing injector concepts.

Supercritical or flashing injection involves operation at conditions where a portion of the liquid flashes to a vapor upon injection. The distinction between the methods is that supercritical injection employs a dissolved gas [2], while flashing injection employs vaporization of the liquid itself. In either case, the fuel is prepared upstream of the injector. The flashing process occurs as the pressure of the liquid is reduced, either within the injector passage or a short distance from the injector exit within the combustion chamber.

The present investigation concentrated on supercritical injection by means of dissolved gases. Figure 1 is a sketch of the concept for a gas turbine combustor. In this case, air is drawn from the inlet of the combustor, compressed, mixed with the fuel, and allowed to dissolve prior to injection.

The potential effect of the supercritical injection is dependent upon the amount of air that can be dissolved in the fuel prior to injection. The first phase of this investigation involved accumulating necessary solubility data and correlating the results using thermodynamic theory [1]. Figure 2 is an illustration of the solubility of air in a typical Jet A fuel blend. Measurements and predictions of solubility are plotted as a function of pressure for two different liquid temperatures. The predictions employ the Soave equation of state for high pressure multicomponent mixtures [1]. The effect of temperature is not very significant over this test range; however, solubility increases almost linearly with pressure, reaching levels of 15-20% dissolved air (molal basis) at pressures of 10-15 MPa.

The predicted solubility of air in Jet A, over a broader range of conditions than Fig. 2, is illustrated in Fig. 3 [1]. It is evident that significant quantities of air can be dissolved in the fuel, particularly at elevated temperatures and pressures. Calculations were also completed to determine the variation of the specific volume of the flow as the dissolved gas mixture was expanded. It was found that the

---

*Numbers in brackets designate references.

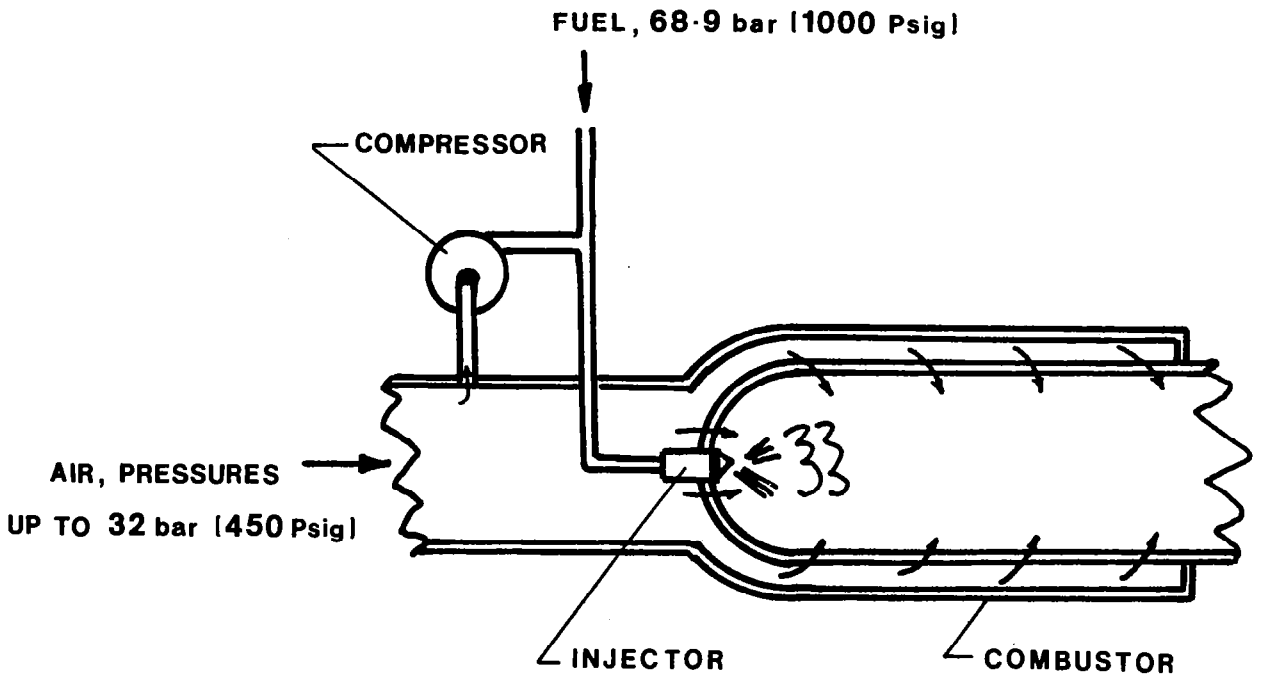

Figure 1. Supercritical injector concept.

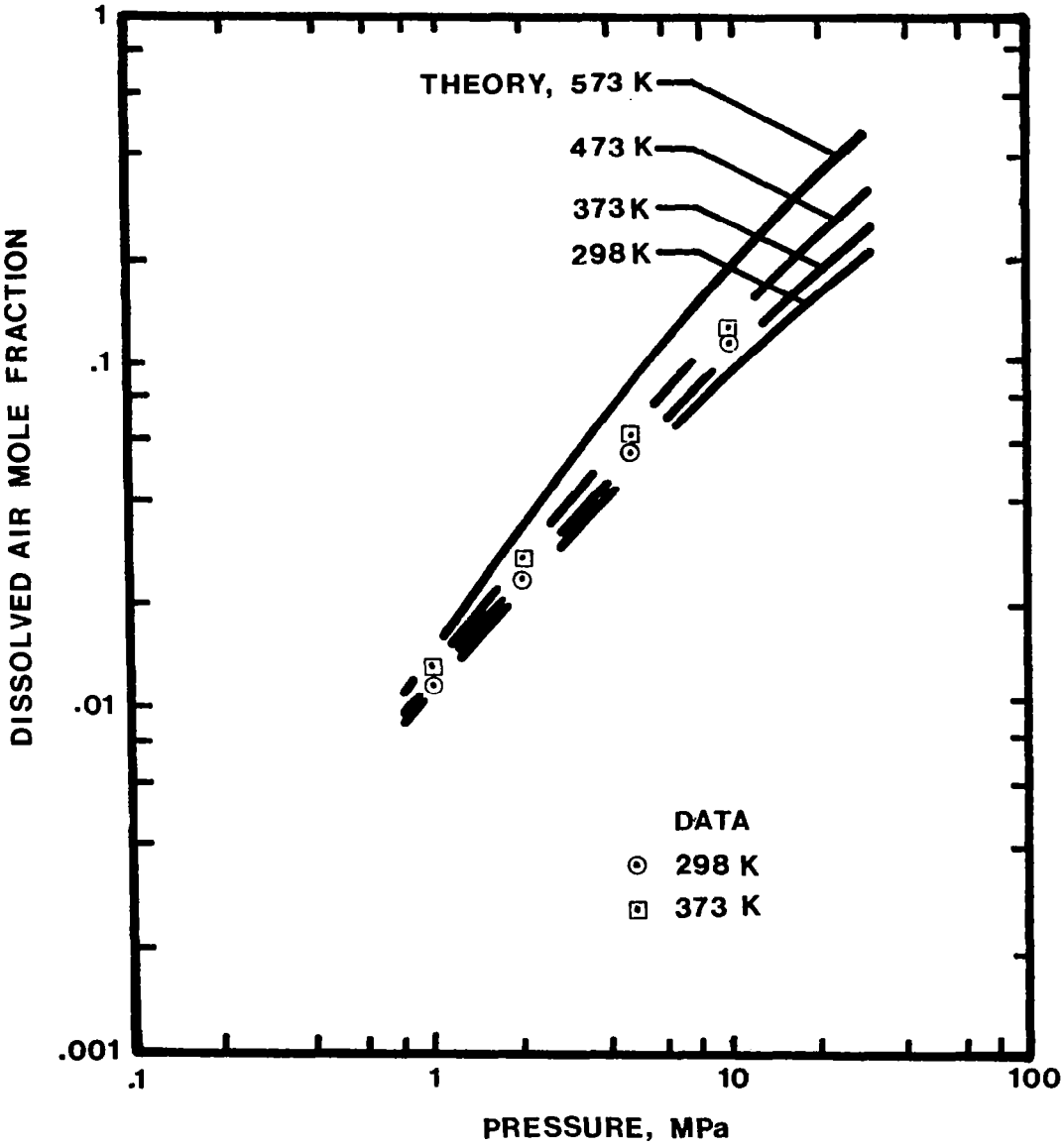

Figure 2. Predicted and measured air solubility in Jet A.

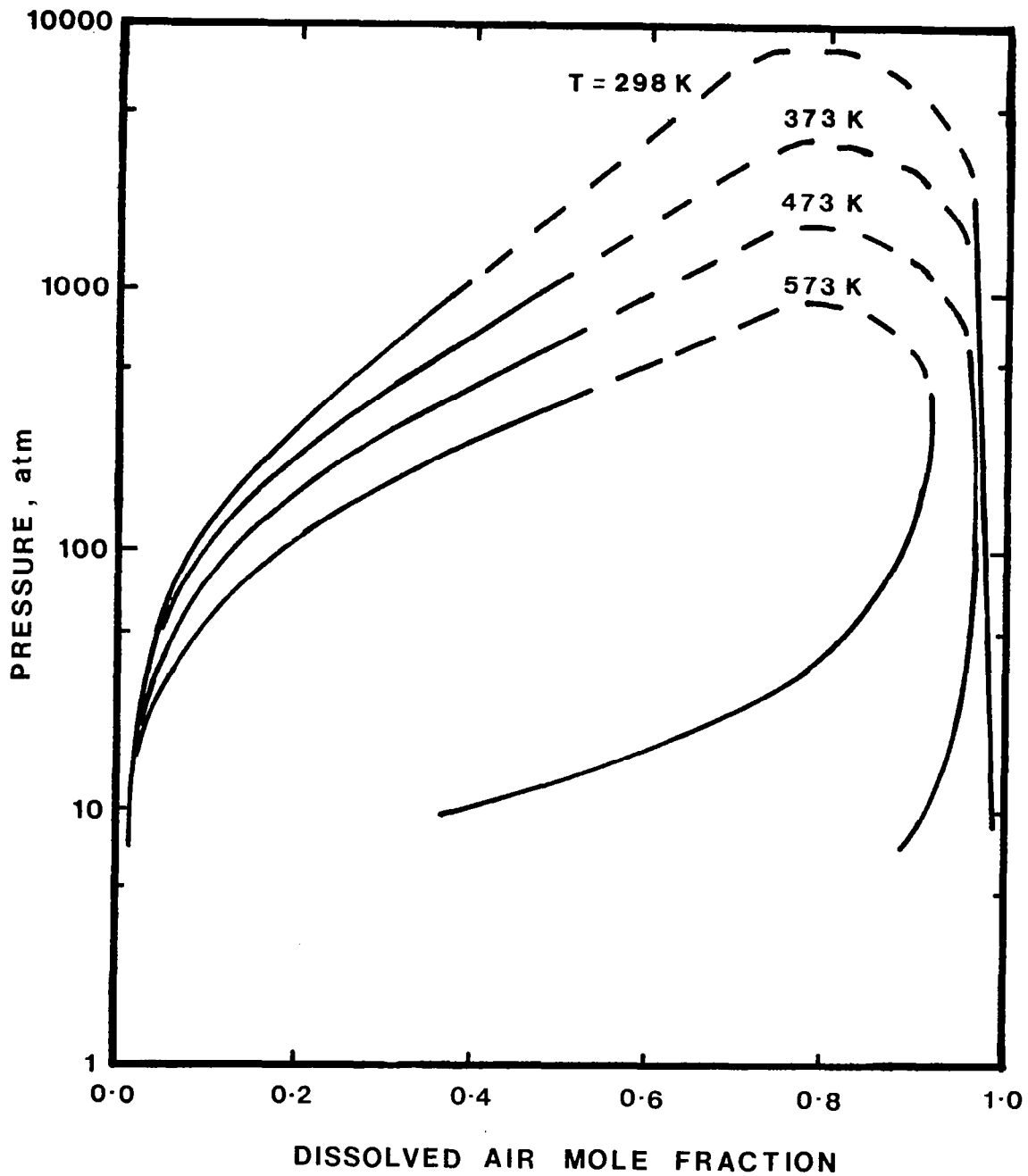

Figure 3. Predicted properties of Jet A/air.

presence of dissolved gas resulted in volume increases of as much as twenty times that of the neat liquid (inlet pressure and temperature 6.9 MPa and 473 K with an outlet pressure of 0.1 MPa). Both dissolved gas and vapor flashing contributed to the volume increase, particularly at higher fluid temperatures [1]. A volume change of this magnitude has the potential of substantially influencing atomization.

Commerical spray cans for paint, deodorants, etc., provide common examples of the effect of flashing dissolved gases for a liquid injection process. In view of this application, several studies of flashing atomization have been reported [4-6]. It is generally agreed that flashing provides a significant reduction of drop sizes in the spray, when compared with conventional liquid injection, improving atomization. Whether similar improvements can be realized with fuel/air mixtures, however, has not been demonstrated. Recent work on the spray angles observed when flashing liquid fuels indicates relatively poor comparison with existing empirical correlations for other liquids [7]; therefore, there is substantial uncertainty concerning the application of available results to fuel/dissolved gas systems.

Aside from the effect of dissolved gases on atomization, the presence of air in the primary zone of a spray flame is known to influence the production of pollutants--particularly soot. Twin-fluid injectors (air blast or air assist) are finding increasing application in gas turbine and aircraft propulsion systems due to this beneficial effect [8]. Dissolved air concentrations illustrated in Figs. 2 and 3 are generally lower than those employed for conventional twin fluid injectors. However, the intimate contact between fuel and air in a dissolved gas system has the potential for better utilization of the air in the injector flow. Whether this is the case, however, must be established.

Having determined the quantities of air that can be dissolved in a typical fuel (Jet A) [1], activities during the current investigation were devoted to determining the influence of dissolved gases and vapor flashing on the atomization and combustion of the fuel. The specific objectives of the current phase of the investigation were:

1. Investigate the atomization properties of flashing liquids, including fuel/dissolved gas (air) systems. Determine and correlate the effect of inlet properties and injector geometry on mass flow rates, Sauter mean diameters (SMD) and spray angles. The injector configuration is limited to straight-hole orifices with no swirl.

2. Examine the combustion properties of flashing injection in an open burner flame. Determine the effect of dissolved air concentrations on flame shape.

All the results of the investigation are described in this report. The report begins with a discussion of atomization, describing first of all the flashing injector concept developed during this study. Theoretical and experimental findings concerning flow regimes, flow rates, drop size distributions, spray angles and liquid flux distributions for this type of injector are then considered. The report concludes with a

description of the combustion properties of flashing injectors--comparing flame shapes for various injector operating conditions.

The authors wish to acknowledge the assistance of D. S. Farrar during the experimental portion of the investigation. J. Tishkoff and D. Hammond of the General Motors Research Laboratories provided valuable advice and calibration data for the Malvern particle analyzer employed during the study.

2. ATOMIZATION STUDY

2.1 Introduction

Atomization properties of dissolved gas systems were examined for injector inlet conditions considered during the earlier investigation of solubility and density properties of dissolved gas mixtures [1]. This includes pressures up to 10.4 MPa, with Jet A-air mixtures. The flashing of pure Freon 11 was also investigated during the present study in order to contrast results for dissolved gas and pure liquid systems.

While swirl is employed for many injector designs, it was felt to be premature to consider this complication at this time. Therefore, testing was limited to straight-hole orifices with no swirl. Measurements of mass flow rates, SMD, spray angle and liquid flux distributions were undertaken using various injector geometries. Models were developed for determining injector mass flow rates, injector exit conditions and SMD for flashing injection processes, in order to assist data correlation and interpretation.

During the course of the research, it was found that the flashing injection process was influenced by the internal geometry of the injector. In particular, the use of an expansion chamber upstream of the injector exit passage was found to substantially improve atomization properties, similar to results obtained by earlier investigators [9-11].

The effect of an expansion chamber is qualitatively indicated in Fig. 4. The top figure indicates conventional pressure atomized injection with no dissolved gas present. In this case, drops are formed by interaction of the flow with gas outside the injector. The second sketch illustrates the process when flashing of vapor or dissolved gas occurs, using a conventional injector. Here, bubbles form within the liquid as it is depressurized and grow similar to bubble growth in homogeneous boiling processes [4-6,12-14]. The radial expansion of the bubbles tends to increase the spray angle, while the formation of relatively thin liquid layers between bubbles reduces SMD. Bubble growth velocities, however, are low; therefore, this approach requires relatively large amounts of vapor production and low flow velocities in order to have a significant impact on spray properties. Bubble growth rates are proportional to liquid thermal diffusivities for flashing pure liquid systems and to liquid mass diffusivities for flashing dissolved

gas systems. Since liquid mass diffusivities are much lower than thermal diffusivities, bubble growth rates in dissolved gas systems are relatively slow in comparison to flashing pure liquids, tending to reduce effects of flashing on atomization properties.

The third sketch in Fig. 4 illustrates flashing injection when an expansion chamber is present upstream of the injector orifice. The flow is partially flashed as it passes through the orifice at the inlet of the expansion chamber. There is a two-phase flow within the expansion chamber which can exhibit a variety of flow regimes (bubbly, slug, churn, annular, annular-mist, etc.) depending upon the mass quality, momentum, passage diameter, and state of flow development [15]. The condition illustrated is an annular-mist flow which would be representative of high momentum conditions with a large volume fraction of gas or vapor. This flow expands through the injector orifice and since it is compressible, choking and external expansion can occur, similar to single-phase flows in nozzles. The liquid in the annulus is drawn into a thin film in the orifice and subjected to a high shear rate by the gas flow, similar to the action of twin-fluid injectors [8]. External expansion and large shear rates tend to increase the jet angle and reduce drop sizes, thus the use of an expansion chamber improves injector performance in these circumstances. The liquid continues to flash as it passes through the injector orifice, which probably also influences the process.

It became evident during the present investigation that the greatest benefits of flashing injection with dissolved gases were obtained when an expansion chamber was present, since the flow in the expansion chamber had adequate time for the relatively slow process of bubble growth to be completed. Therefore, the study was largely concerned with the properties of flashing injection with an expansion chamber within the injector.

In the following, the arrangement of the atomization apparatus and instrumentation is described first. This is followed by a description of the theoretical models used to analyze flow regimes in the expansion chamber, the flow properties of the injector, and the drop size distribution in the spray. This section of the report concludes with a description of experimental and theoretical results concerning flow regimes, injector flow rates, spray SMD, spray angles and the distribution of liquid flux within the spray.

2.2 Experimental Methods

2.2.1 Apparatus

The previous discussion suggests that properties of the expansion chamber (diameter, length, pressure, flow mass quality and flow rate) can influence flashing injector performance, since these parameters affect flow regimes of two-phase flow in tubes [15]. Therefore, a universal injector was designed for the tests, where expansion chamber geometry could be changed with little difficulty.

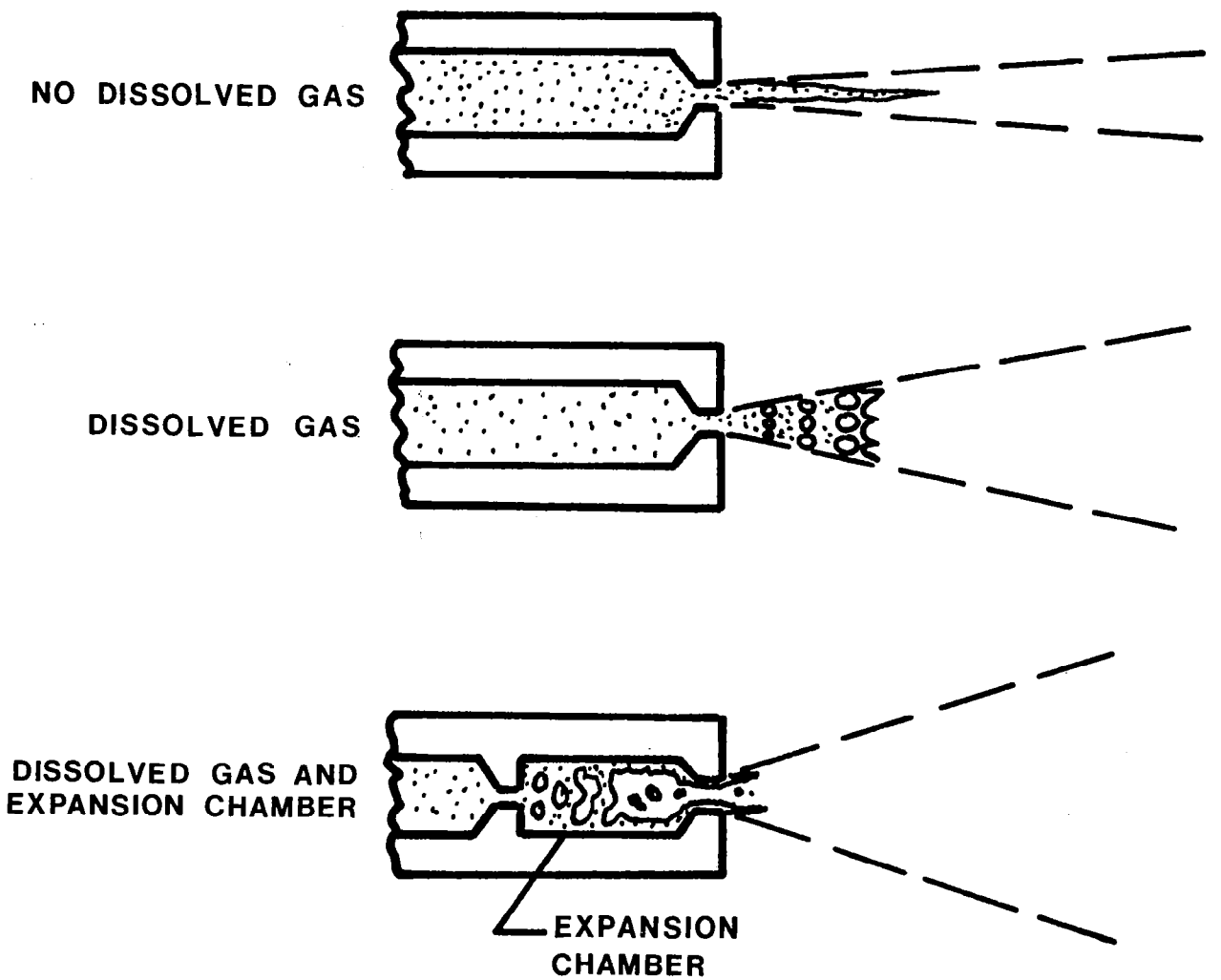

Figure 4. Flashing injection process.

A sketch of the universal flashing injector appears in Fig. 5. While the injector orifice was replacable, the tests reported here employed a straight hole passage with a diameter of 0.2 mm and a length-to-diameter ratio of two. The orifice at the upstream end of the expansion chamber was variable--consisting of a bank of ten orifices, constructed from watch jewels, having diameters in the range 0.07-0.46 mm. Several different expansion chamber geometries were examined--their configuration is illustrated in Fig. 6. Tests were primarily conducted using configuration A, which involved no insert to reduce the volume of the expansion chamber, yielding the configuration illustrated in Fig. 5. During preliminary tests, a fourth configuration was also considered where a valve acted as the flow restriction with a 300 mm length of 4.6 mm ID tubing between the valve and the injector block.

A sketch of the experimental apparatus appears in Fig. 7. Vertical downward injection was employed for most of the tests, except when the Malvern particle size analyzer was used when injection was horizontal. The injector operated in the open with the flow removed by an exhaust vent located downstream of the measuring station. The vent caused the spray to be within a coflowing air stream having a velocity less than 1 m/s. Since liquid velocities were relatively high, greater than 10 m/s, the injector was essentially operating in a stagnant air environment.

The fuel was saturated with air directly in the fuel tank, similar to the earlier study of solubility in this laboratory [1]. This involved partially filling the tank with fuel, pressurizing the tank with air to the desired saturation pressure, and then manually agitating (shaking) the tank to achieve equilibrium solubility levels.

The saturated air pressure within the fuel tank provided the driving pressure for flow through the injector. The flow was initiated by manually opening the shut-off valve in the line between the fuel tank and the injector.

Some tests were conducted with flashing Freon 11. In this case, the fuel tank and the line between the fuel tank and the injector were wrapped with heating coils and insulated. Temperatures of the fuel tank and tubing were measured with several chromel-alumel thermocouples spot-welded to their surfaces. The liquid was placed in the fuel tank and pressurized with nitrogen, but the tank was not agitated so that the bulk of the liquid contained negligible amounts of dissolved nitrogen. The tank and line were then heated to the desired level by adjusting the power of the heater coils with a Variac. Pressurizing gas was vented from the upper portion of the tank during heating in order to compensate for the increased vapor pressure of the liquid so that the desired injector pressure could be maintained. Once the system had stabilized at the correct temperature and pressure, the test was initiated by opening the shut-off valve in the injector supply line.

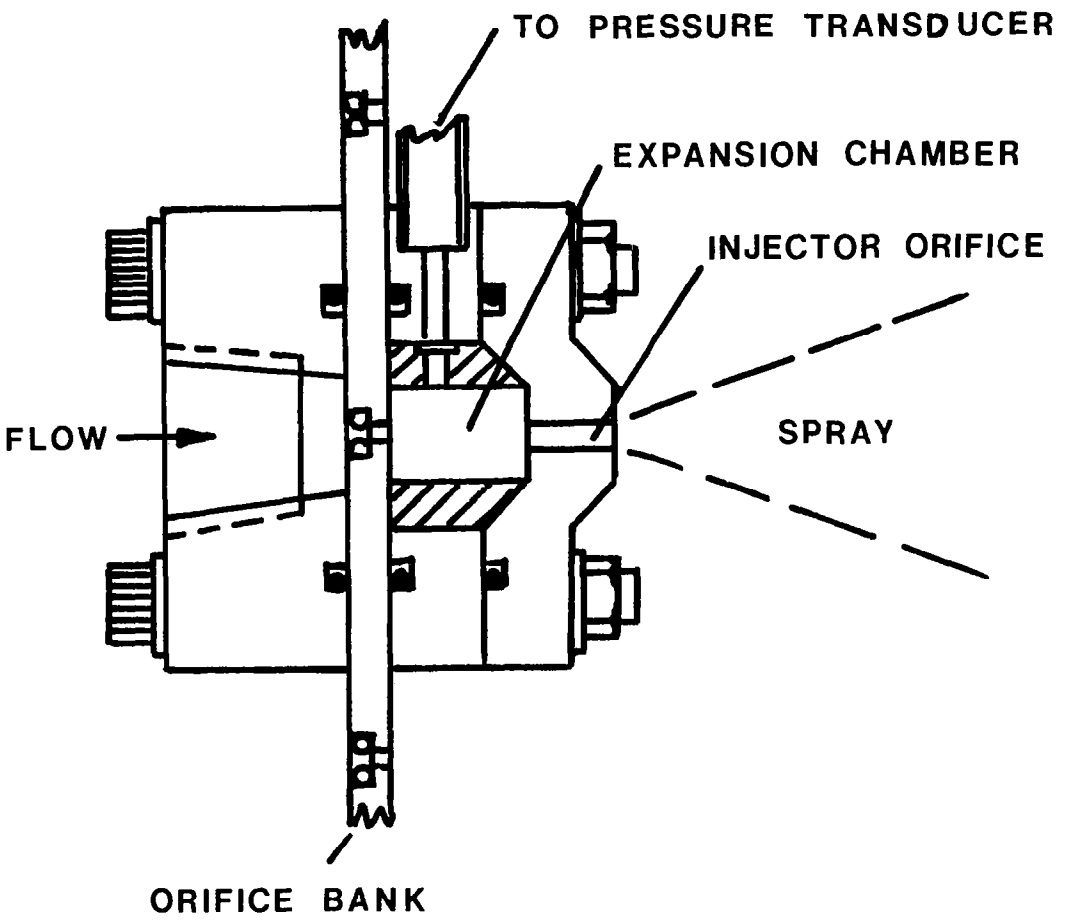

Figure 5. Experimental flashing injector.

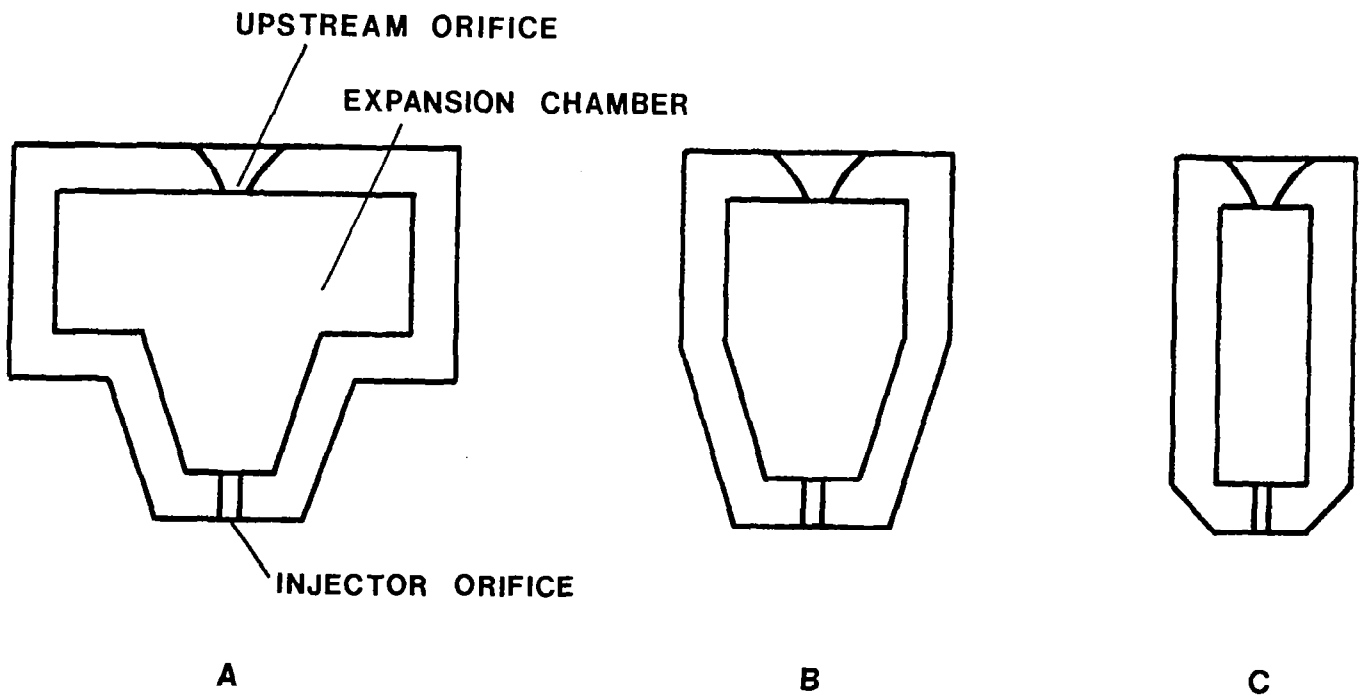

Figure 6. Expansion chamber geometries.

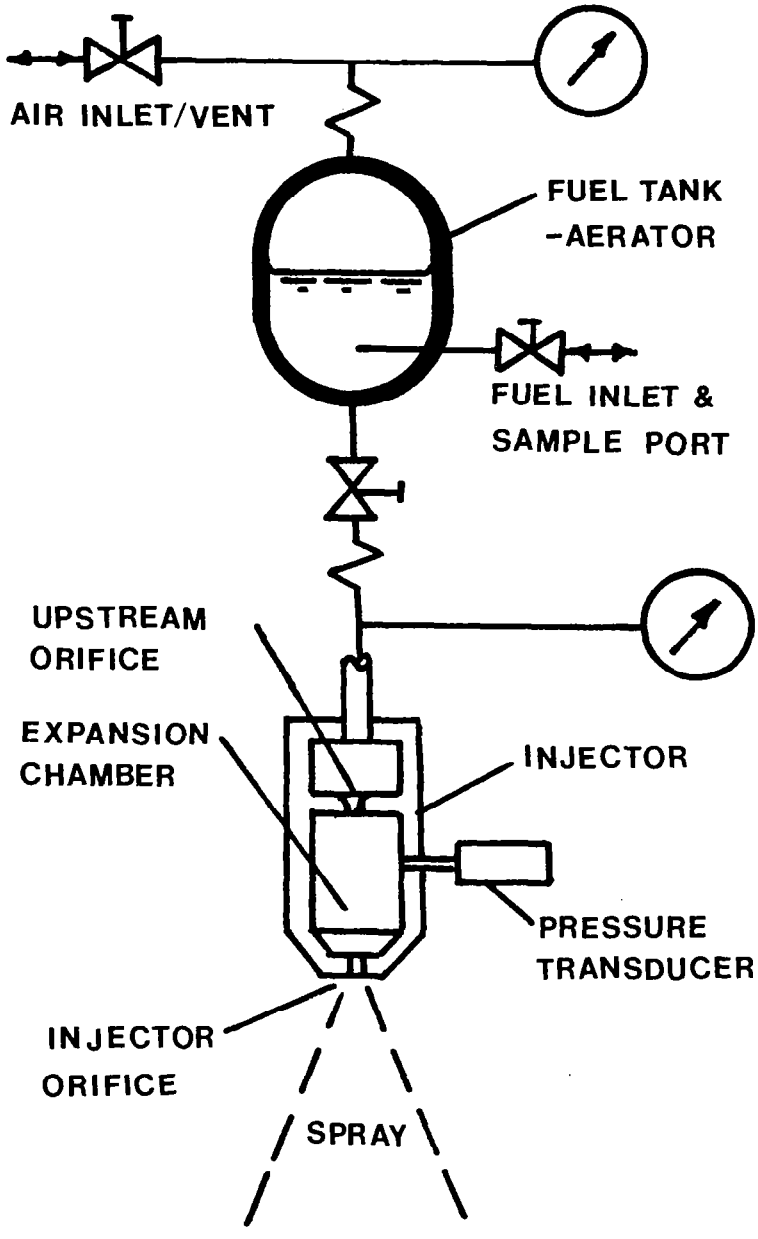

Figure 7. Flashing injector apparatus.

2.2.2 Instrumentation

Pressures were measured in the fuel tank and the expansion chamber. The fuel tank pressure was measured with Heisse absolute pressure gauges (0.1% accuracy, 0-10.3 and 0-51.7 MPa ranges, using two gauges). The expansion chamber pressure was measured with a Validyne No. DP15TL transducer and model CD12 read-out unit. The Validyne pressure measurements were calibrated using the Heisse pressure gauges, which had been calibrated earlier using a dead weight tester.

The fuel tank and fuel line temperatures were measured with 26 gauge chromel-alumel thermocouples whose junctions were spot-welded to surfaces. A sheathed, chromel-alumel thermocouple, 1.6 mm OD was also placed in the fuel flow, just upstream of the injector. The thermocouples were provided with an ice bath reference junction. Thermocouple output was measured with a Leeds and Northrup, model 8686, null potentiometer as well as a Hewlett Packard, model 419A, null voltmeter.

Dissolved gas levels were measured in the same manner as Ref. 1. This involved drawing a sample into a graduated tube at atmospheric pressure and allowing the air to come out of solution. The volume of gas and liquid in the sampling tube, then yields the dissolved gas level since the vapor pressure of the liquid and the solubility of the air in the fuel are both negligibly small at normal temperature and pressure, c.f., Fig. 2 and Ref. 1.

Injector flow rates were determined by measuring the time required for a known mass of fuel, placed in the fuel tank, to pass through the injector. The total time of flow for these measurements was several minutes, since fast acting valves were not used to initiate injector flow.

The spray was photographed using a Graphlex 4 x 5 still camera with Polaroid Type 52 film at a shutter speed of 1/50 s. The camera lens (f/7.5, 203 mm focal length) was located on an extension to provide a 7.5:1 primary magnification of the spray. The spray was illuminated from the front using two 750W quartz lamps.

The spill-over technique was used to measure the distribution of liquid flux in the spray [16]. This involved twelve glass tubes, 8 mm ID x 10 mm OD, closed at the bottom and ground with a taper at the top, which were placed in a rack within the spray. When the entrained air in the spray passed over each tube, the bulk of the liquid was captured (except for the smallest drops) and collected in the bottom of the tube. Sample collection for a fixed period of time allowed the liquid flux to be measured volumetrically. The performance of this system was influenced by the capture efficiency of the tubes. Comparison of total liquid flow rates measured at the fuel tank and computed from the liquid flux measurements of the spill-over tubes, indicated a collection efficiency of 70-90% for present test conditions.

Three methods were employed to measure drop sizes: the drop impaction technique developed during earlier research on sprays in this laboratory [17,18]; a Malvern Particle Size Analyzer, which is based on the light scattering properties of the particles; and a second light scattering method, based on an approach developed by Dobbins, et al. [19].

A sketch of the droplet impactor system appears in Fig. 8. Glass slides having a width of 5 mm are coated with magnesium oxide and placed in the holder illustrated in Fig. 8. The shutter mechanism provides a means of exposing the slide to the spray for a short time interval. The shutter consists of a 6.35 mm hole drilled in a pneumatically driven slider. When the slide is exposed to the spray, the drops leave an impression in the magnesium oxide coating proportional to their size. The experimentally verified uniform correction factor of 1.12 was used for the ratio of impression diameter in the magnesium oxide coating to droplet diameter, c.f., May [20]. After exposure, the slide is placed under a microscope where the impressions are sized and counted. Several thousand drops were counted in order to provide a statistically significant indication of the spray size distribution. The collection efficiency of the system varies with drop size and velocity, with the smallest drops passing around the impactor [18]. The present measurements were not corrected for this effect, however, since local gas velocities were not measured. It is estimated that the collection efficiency is greater than 85% for drops larger than 15 μm.

The Malvern Particle Size Analyzer, model 2200, was used for the bulk of the drop size measurements. This instrument works on the principle of Fraunhofer diffraction from particles illuminated by a laser beam as described by Swithenbank, et al. [21]. The major components of the instrument are shown schematically in Fig. 9. The transmitter is a 2 mW, HeNe laser, with a spatial filter and beam expander to provide a 9 mm diameter collimated beam. The detector arrangement used during the present experiments employed a 300 mm diameter focal length collecting lens which focused the light scattered from particles in the beam path on a photodiode detector having 30 concentric rings. The signal from each ring is sampled and processed to yield the size distribution of the spray as discussed by Swithenbank, et al. [21]. While specific size distribution functions can be assumed as part of the data processing--for example Rosin-Rammler or log normal--processing in the present case employed a model-independent procedure which yielded the weight percentage of the spray in 15 size ranges. This data was then processed independently to obtain spray statistics such as Sauter mean diameter (SMD) on a computer.

The Dobbins, et al., [19] method of measuring SMD was used during the initial stages of the investigation. This method is also based on light scattering from the path of a laser beam. The laser source was a 5 mW, HeNe laser, which passed through a spatial filter and beam expander to form a collimated 7.5 mm diameter beam. After passing through the spray, the scattered light was collected with an 85 mm diameter, 600 mm focal length lens. The scattered light distribution was measured in the focal plane of the lens using a photomultiplier

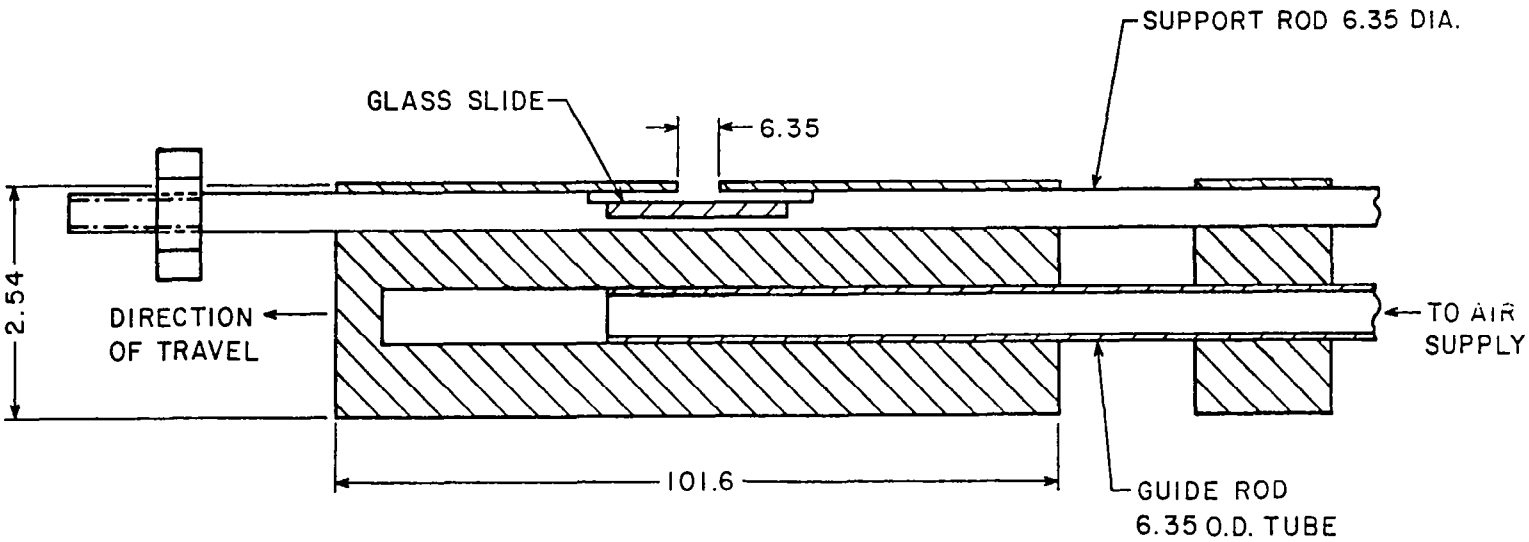

Figure 8. Sketch of the droplet impactor.

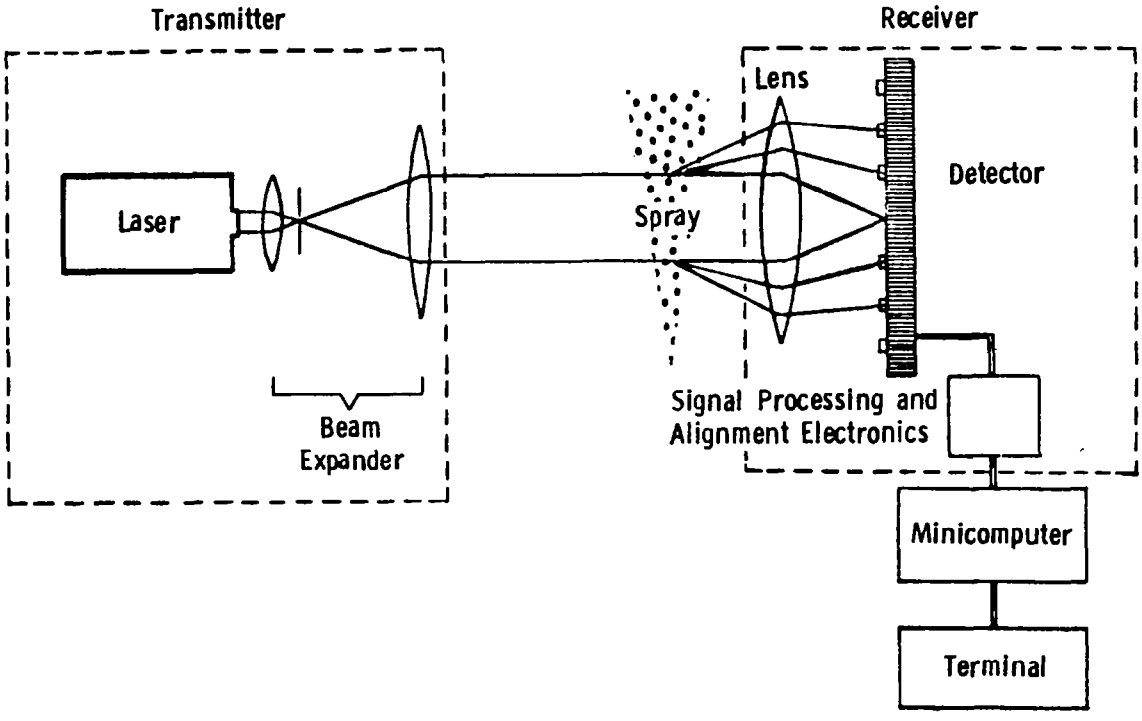

Figure 9. Sketch of the particle size analyzer.

having an aperture of 0.2 mm diameter. The photomultiplier was mounted on a linear positioner to yield the intensity of scattered light as a function of radial position. The signal to noise ratio of the system was improved by chopping the laser beam while employing a high pass filter on the detector output. The variation in scattered light intensity yields the SMD as described in Ref. 19.

2.2.3 Calibration of Drop Sizing Instruments

The slide impactor system was used following the same procedures as Ref. 17 and no additional calibration of this device was necessary.

The Malvern Particle Size Analyzer operates on fundamental scattering principles; therefore, the manufacturer states that no calibration is necessary. Nevertheless, the instrument was calibrated in order to gain confidence in its use. Two calibration experiments were conducted. The first evaluation considered a sample of Dow latex spheres of known size using a procedure developed by Hammond [22]. The spheres are specified by the manufacturer to have a mean diameter of 25.7 microns with a standard deviation of 10 microns. This material was delivered as a concentrated aqueous solution which was diluted so that the single-scattering limit of the instrument was still applicable. The diluted suspension was placed in a 3 mL spectrometer sample cell providing a 10 mm beam path through the suspension. The dilution was adjusted so that the on-axis attenuation of the laser beam was 20%--a typical value for measurements in sprays.

The results of the size determination of the latex spheres are illustrated in Fig. 10. Three distributions are shown, the size distribution specified by the manufacturer, the distribution measured by Hammond [22] and the present measurement. Different samples were used in the three determinations, nevertheless, the agreement between the measurements is quite good.

The second calibration involved the measurement of drop size distributions for the ASTM "round robin" injector. Present measurements were compared with earlier results obtained by Hammond [23], Harding [24] and Tishkoff [25]. This injector is a Delevan type WDA-2.0-80°. The standard operating condition involves a flow of water at room temperature through the injector with a supply pressure of 267 kPa. This injector yields a spray with a hollow cone pattern.

The comparison of SMD measurements at various points in the water spray is illustrated in Fig. 11. Results are shown for Hammond [23] using a Malvern instrument, Harding [24] using both an imaging system and a Malvern instrument, Tishkoff [25] using an imaging system and the present Malvern measurements. Agreement between the present measurements and the results of Hammond is excellent; however, only fair agreement is obtained for all the systems combined. Hammond points out that these discrepancies can be attributed to large scattering effects in the imaging data, line-of-sight averaging effects, and physical differences in the experimental arrangements, e.g., different

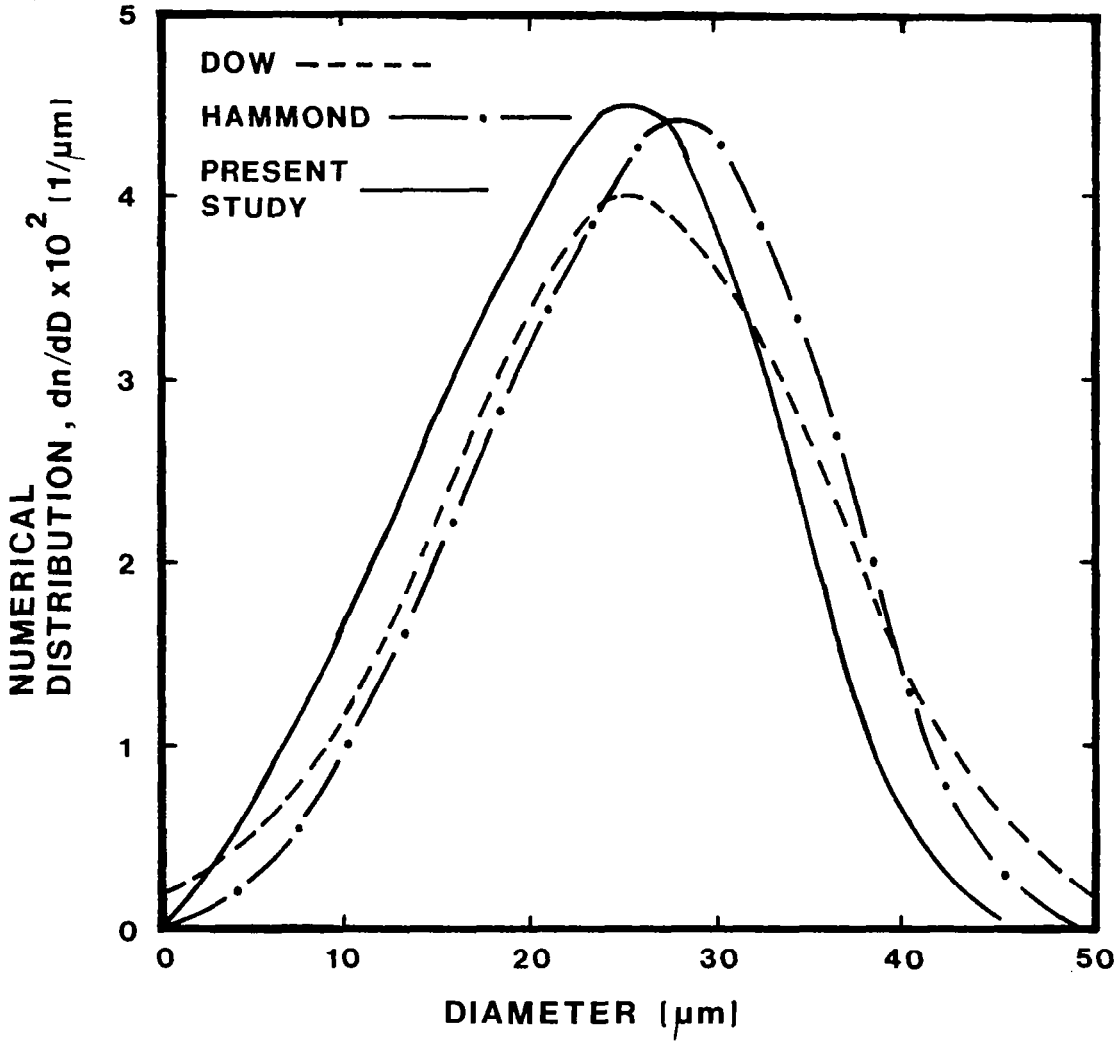

Figure 10. Calibration of particle size analyzer with Dow latex spheres.

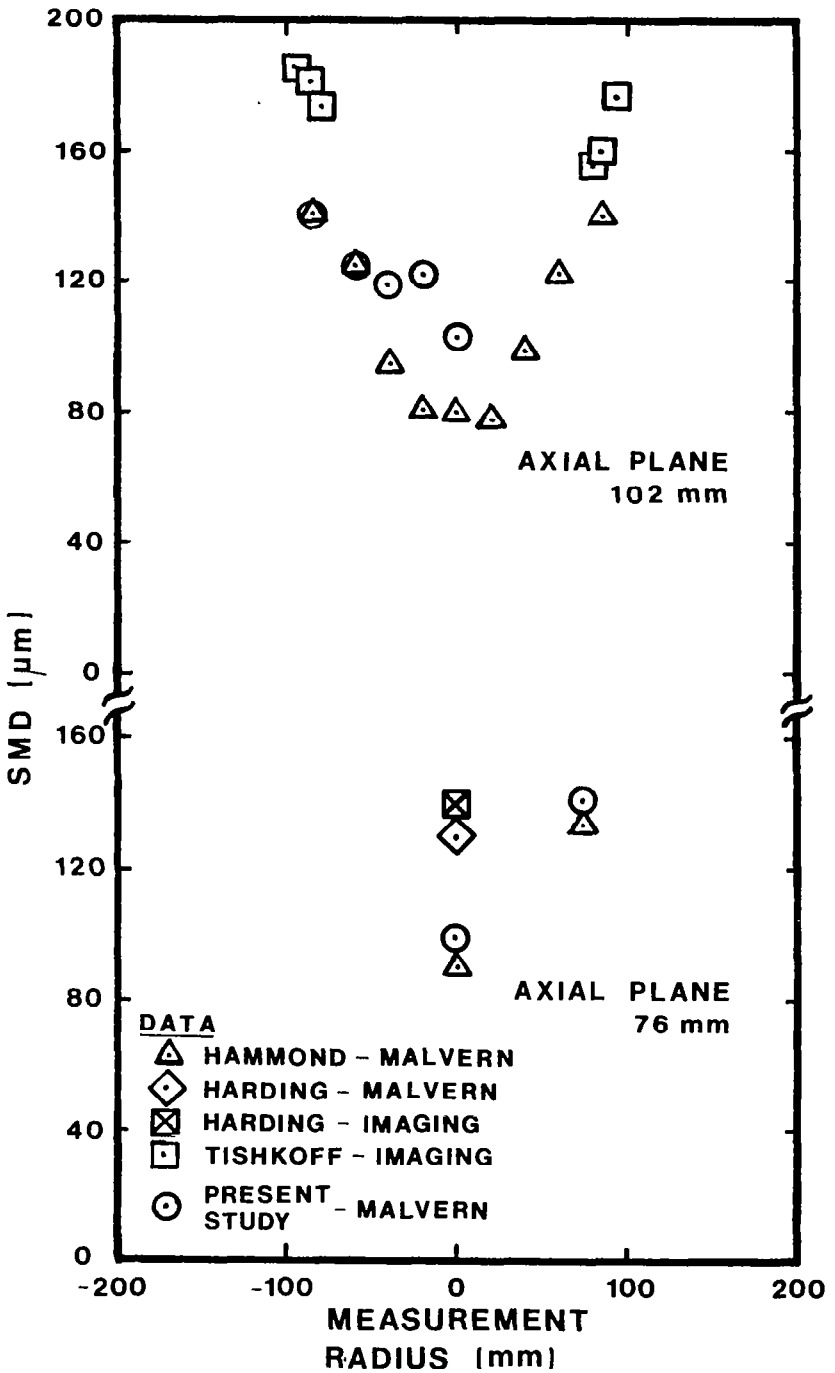

Figure 11. Calibration of particle size analyzer using ASTM "Round Robin" Nozzle.

injectors and the fact that coflow conditions varied for the results illustrated in Fig. 11. Based on the calibration results, it was concluded that the present Malvern measurements yielded reasonably accurate results which could be reproduced by others.

The first calibration of the light scattering procedure of Dobbins, et al., [19] employed a monodisperse stream of drops, having a diameter of 42 microns, from a Berglund-Lieu Particle Generator. For monodisperse particles, the illumination profile is a ringed diffraction pattern, allowing the determination of particle size by measuring the angle subtended by any one of the dark rings [19]. In this case, the light scattering method yielded a diameter of 44 microns, providing good agreement.

A second calibration of the Dobbins, et al., [19] method involved measurements with the test injector, using Jet A fuel containing no dissolved gas at an injector pressure of 6.87 MPa, measured at a distance of 1000 mm from the injector exit. Slide impaction measurements were taken at this location, counting 12000 drops over the cross section of the spray to yield a SMD of 55 microns. In this case, the light scattering method required a determination of the on-axis component of scattered light intensity which proved to be very difficult for our arrangement due to the presence of the intense unscattered beam. As a result of this uncertainty, measured values of SMD scattered from the calibrated value in an inconsistent manner; therefore, this approach was only used to a limited degree, while most of the drop size measurements were obtained with the Malvern Analyzer.

2.3 Theory

Theoretical considerations were limited to three aspects of flashing injection: flow regimes in the expansion chamber, the flow properties of the injector, and the drop size distribution of the spray.

2.3.1 Expansion Chamber Flow Regimes

Expansion chamber flow regimes were analyzed in order to indicate the potential topography of the two-phase flow entering the injector passage. The main assumption made during this analysis was that the flow in the expansion chamber was in thermodynamic equilibrium, i.e., that the dissolved gas had sufficient time to come out of solution and equilibrate within the flow passage. For present test conditions, flow residence times in the expansion chamber were in the range 0.1-0.6 ms; therefore, this assumption is reasonable.

The second major assumption of the flow regime analysis was that the flow was fully developed. For present test conditions, length-to-diameter ratios for the expansion chamber were in the range 1.4-3.0. Since two-phase flows generally require length-to-diameter ratios in excess of 100 to become fully developed, this assumption is not satisfied for present test conditions; therefore, the following estimates are primarily indicative of the direction in which the flow is evolving.

Injector behavior was independent of orientation (horizontal or vertical); therefore, flow regimes for both configurations were considered. Collier [15] reviews methods for estimating flow regimes. For horizontal flow, Baker [26] presented the earliest flow regime map, which is still widely used for adiabatic flows. In a later study, Mandhane, et al., [27] propose a different empirical method of correlation based on their own measurements. A more rational method of estimating flow regimes, which are based on phenomenological analysis of flow regime transitions, is described by Taitel and Dukler [28]. This method successfully correlates the Mandhane, et al., [27] measurements and is recommended for general use [15]. Similar flow regime maps are available for vertical flows, e.g., Hewitt and Roberts [29] for upflow and Oshinowo and Charles [30] for downflow.

The Taitel and Dukler [28] method will be considered in greatest detail in the following. For present injector conditions, wavy and stratified flows were not a factor; therefore, only transitions between annular, bubbly and intermittent (plug/slug) flow regimes were considered. These transitions are determined as a function of the Lockhart-Martinelli parameter

$$X = \left[\left(\frac{dp}{dz}F\right)_f / \left(\frac{dp}{dz}F\right)_g\right]^{1/2} \tag{1}$$

The frictional pressure gradients appearing in Eq. (1) are evaluated for liquid or gas, alone, flowing in the tube, i.e.

$$\left(\frac{dp}{dz}F\right)_i = -2f_i G_i^2/(\rho_i D) \quad , \quad i = f \text{ or } g \tag{2}$$

where f_i is the Fanning friction factor. Taking values for a smooth round tube, the friction factor was found from

$$\begin{aligned} f_i &= 16/Re_i \quad , \quad Re_i < 2300 \\ &= 0.046/Re_i^{0.2} \quad , \quad 2300 < Re_i < 10^5 \end{aligned} \tag{3}$$

and

$$Re_i = G_i D/\mu_i \quad , \quad i = f \text{ or } g \; . \tag{4}$$

The mass velocity of each phase is given by

$$G_f = (1 - x)G \quad , \quad G_g = xG \; . \tag{5}$$

The second parameter required to determine flow regime transitions is

$$T = [(\frac{dp}{dz} F)_f / ((\rho_f - \rho_g) g \cos \theta)]^{1/2} \quad (6)$$

where θ is the inclination of the tube.

The parameters X and T depend on the amount of gas dissolved in the liquid (represented by the saturation pressure within the tank), the pressure within the expansion chamber, the diameter of the expansion chamber and the flow rate through the injector. For present test conditions, flow rates were measured for various injector inlet pressures and solubility conditions were known from earlier work [1], yielding gas and liquid mass flow rates in the expansion chamber.

Present operating conditions within the expansion chamber are plotted on the Taitel and Dukler [28] flow regime map in Fig. 12. Present tests with dissolved gas involved Jet A fuel saturated with air at 3.45, 6.87 and 10.34 MPa, for a range of expansion chamber pressures. The operating conditions of the expansion chamber are seen to be generally in the bubbly flow region, tending toward annular flow at low values of p_e/p_u.

Table 1 is a summary of estimated flow regimes in the expansion chamber, utilizing the criteria of Refs. 26-30. For the horizontal conditions, the flow regime was bubbly--but near the annular flow transition, similar to Fig. 12--for all the methods examined. Wispy annular flow and froth annular flow was indicated for vertical upflow and downflow.

Flow development effects and the acceleration of the flow at the downstream end of the expansion chamber also influence flow properties in the injector passage. It is likely that the gas first appears as bubbles which require some time to evolve to an annular flow in instances where annular flow is indicated for fully developed conditions. Conversely, the turning of the flow as it converges into the injector passage results in centrifugal forces which causes liquid to accumulate along the walls of the passage--tending to make the flow annular.

In view of the uncertainties, the flow at the exit of the expansion chamber cannot be determined conclusively. Bubbly flow is indicated for horizontal configurations; however, flow development at the injector inlet and the nearness of the transition boundary results in a potential for annular flow.

It is very unlikely that flow regimes within the injector orifice correspond to fully developed regimes for comparable conditions. However, making this evaluation suggested that the flow regimes at the orifice exit were similar to those listed in Table 1 for the expansion chamber.

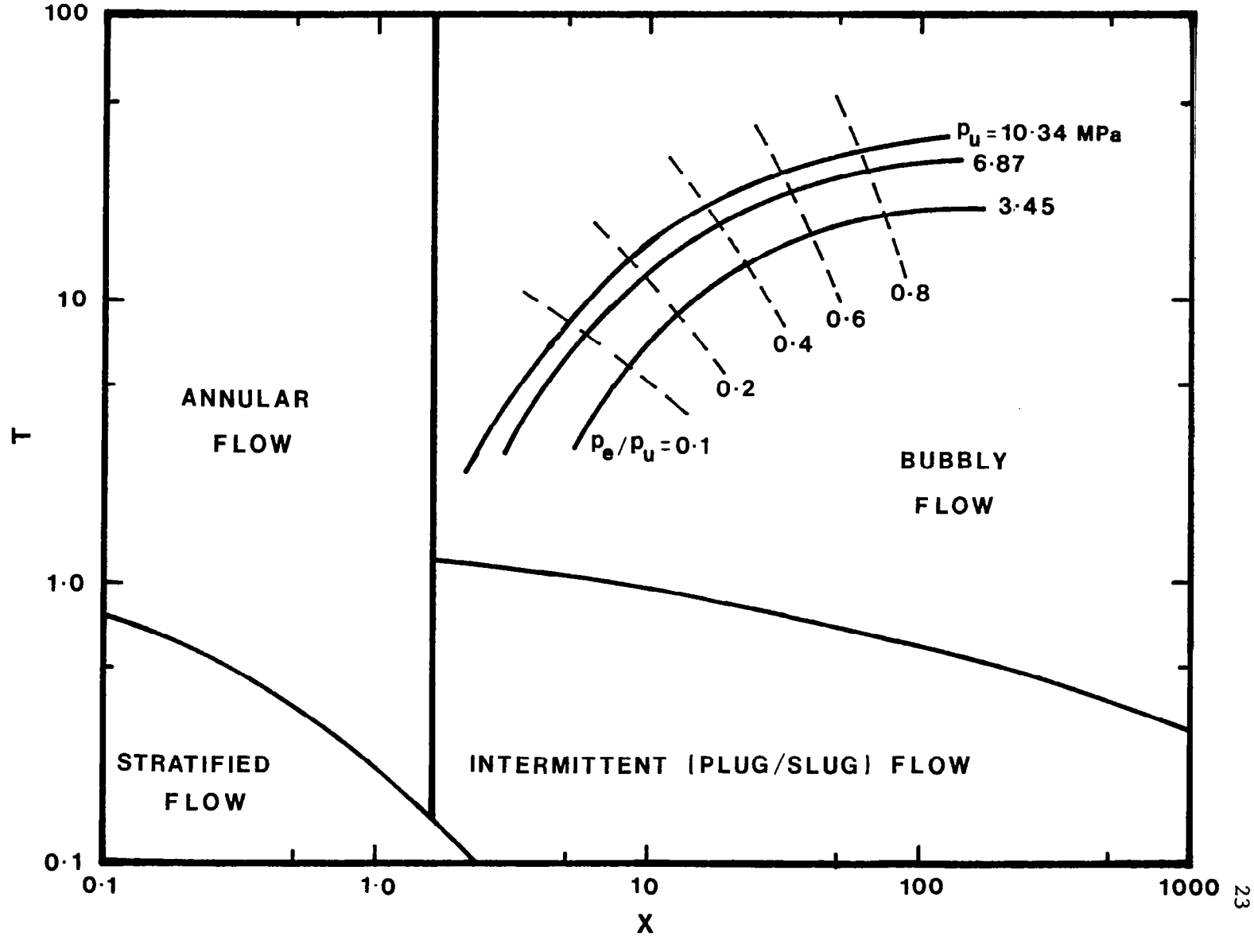

Figure 12. Expansion chamber flow regime map for Jet A fuel saturated with air at p_u.

Table 1 Summary of Flow Regimes[a]

Method	Orientation	Flow Regime
Baker [26]	horizontal	bubbly (froth), annular (dispersed)
Mandhane, et al. [27]	horizontal	bubbly, bubbly annular
Taitel and Dukler [28]	horizontal	bubbly, bubbly annular
Hewitt and Roberts [29]	vertical-upflow	wispy annular
Oshinowo and Charles [30]	vertical-downflow	froth annular

[a]Jet A saturated with air at 3.45-10.34 MPa, p_e/p_u = 0.1-0.9.

2.3.2 Injector Flow Rate Model

Vapor appears when a saturated liquid is depressurized. Therefore, the flow characteristics of flashing injectors are complicated by two-phase flow phenomena. The objectives of the present analysis are to provide the mass flow rate and expansion chamber conditions (mass fraction of vapor, pressure and temperature) as a function of the size of the flow passages at the inlet and outlet of the expansion chamber. A second objective is to provide an estimation of conditions at the exit of the injector orifice, since properties at this point have a strong influence on the atomization and spread of the spray.

The flow properties of the upstream orifice at the inlet of the expansion chamber were determined by neglecting flashing in the orifice passage. This is reasonable, since the residence time of the flow in the orifice is small (typically less than 20 μs). Liquids with dissolved gases remaining in solution have properties which are relatively independent of pressure; therefore, the flow through this orifice was modeled as an incompressible liquid. Under these assumptions, conventional analysis of flow through an orifice yields

$$\dot{m} = C_{fu} A_u (2\rho_f (p_u - p_e))^{1/2} \tag{7}$$

where C_{fu} is the flow coefficient of the orifice. The flow coefficient for the orifices used during the present tests was determined by standard flow calibrations with Jet A containing no dissolved gas.

The residence time of the flow in the expansion chamber was relatively long for present test conditions (greater than 0.2 ms), however, estimated heat transfer rates were small. Therefore, it was assumed that the flow reached the equilibrium state for adiabatic flashing, with negligible kinetic energy, at the entrance of the injector orifice. Conservation of energy yields

$$h_u = (x\, h_g + (1-x)\, h_f)_e \tag{8}$$

while equilibrium between the phases requires

$$F_f = F_g$$

where the h_i and F_i are known from the thermodynamic equation of state of the system. These properties are provided in Ref. 1 for the Jet A/air system and in Ref. 31 for Freon 11. Given the upstream condition and the

expansion chamber pressure, Eqs. (8) and (9) are sufficient to determine the mass quality and temperature of the fluid at the exit of the expansion chamber, recalling that the assumption of thermodynamic equilibrium implies that the temperature of both phases is the same.

Three different approaches were examined to determine the flow properties of the injector orifice at the downstream end of the expansion chamber. The first approach involved application of the empirical method for treating two-phase flows in nozzles and orifices developed by Chisholm [32], which is also discussed by Collier [15]. This method did not yield a satisfactory correlation of the present data. The primary difficulty was that pressure ratios across the injector orifice for present test conditions were far in excess of the values considered by Chisholm [32].

The two other methods employed for the analysis of flow in the injector orifice involved considering the limits of separated flow, with negligible interphase transport rates, and locally homogeneous flow, with infinite rates of interphase transport. A sketch of the separated flow model appears in Fig. 13. For purposes of analyzing the flow, the orifice is approximated as a converging nozzle. The flow can be choked in this arrangement, which is the case shown in Fig. 13. The flow is assumed to be annular, with negligible entrainment of liquid by the gas phase. This is partially justified by the results of Section 2.3.1, which showed that conditions within the expansion chamber were either in or near the annular flow regime. Other major assumptions of the separated flow analysis are as follows:

i. The flow is steady and one-dimensional, i.e., the pressure and the velocities of each phase are uniform over the cross section of the flow, although the velocities of the two phases are generally not the same.

ii. Exchange of heat, mass and momentum between the phases is negligible.

iii. Wall friction is negligible.

iv. The dissolved gas content of the liquid phase is frozen at the expansion chamber condition, i.e., the mass quality x is constant.

v. The liquid is incompressible, implying that its temperature is the same as in the expansion chamber.

vi. The gas flow is treated as the adiabatic and frictionless (isentropic) expansion of an ideal gas with constant specific heats.

With these assumptions, the gas flow is subject to choking (sonic exit velocity) at sufficiently high pressure ratios across the orifice. When choking occurs, the pressure at the exit of the orifice is greater than the ambient pressure, similar to choked single-phase flow of a compressible gas in a nozzle, and final adjustment to the ambient pressure takes place beyond the orifice exit. Observations of flashing injectors suggested that choked flows with external expansion were present at some conditions, as evidenced by unusually large spray angle.

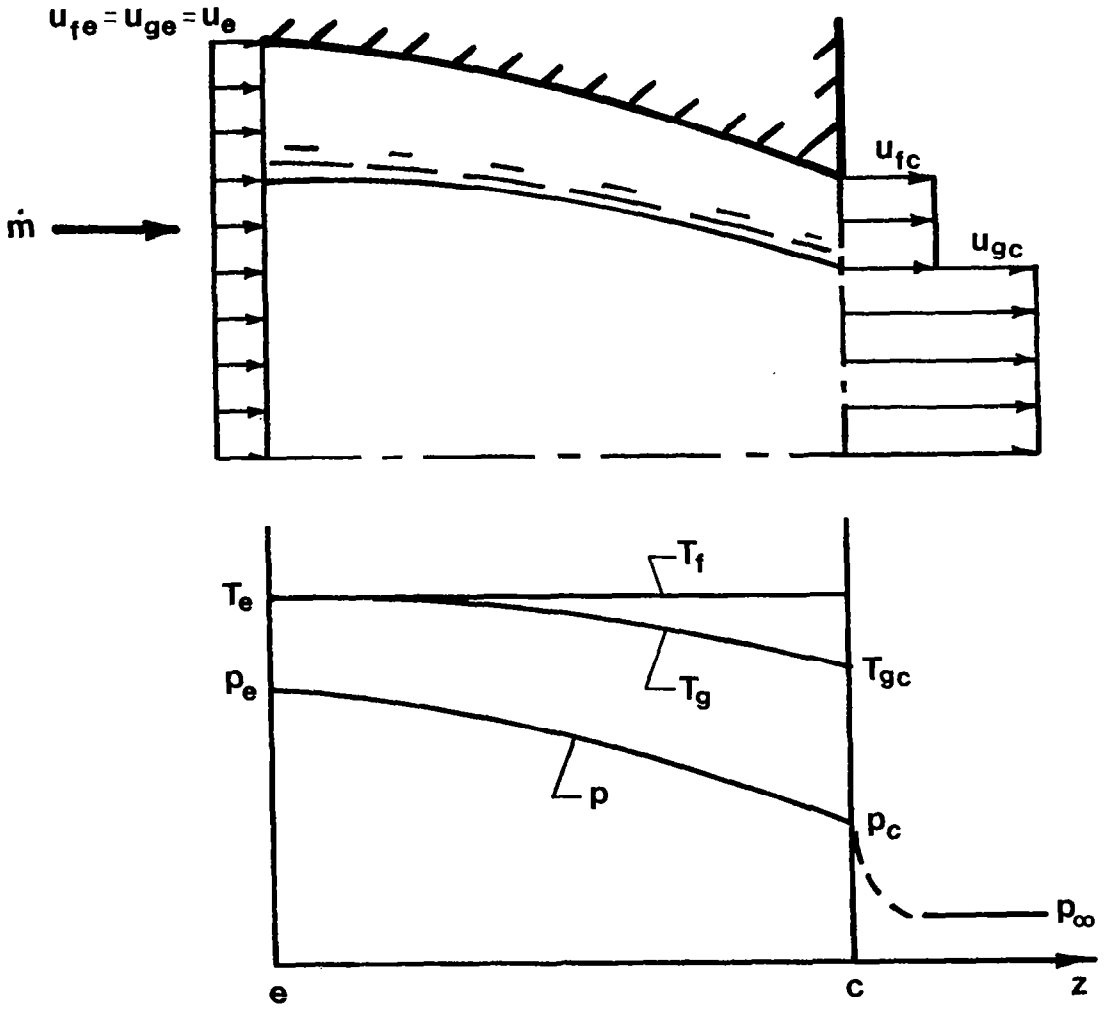

Figure 13. Sketch of the separated flow model of the injector orifice.

The sonic pressure ratio for the gas flow is given by [33]

$$\frac{p_{cs}}{p_e} = \left(\frac{2}{k+1}\right)^{\frac{k}{k-1}} \tag{10}$$

If $p_\infty \geq p_{cs}$, the flow at the exit of the orifice is subsonic and $p_c = p_\infty$, while if $p_\infty < p_{cs}$, the flow is sonic (choked) at the exit of the orifice and $p_c = p_{cs}$. In either event, properties of the liquid and gas phases at the exit of the orifice are as follows [33]:

$$\rho_{fc} = \rho_{fe} \tag{11}$$

$$T_{fc} = T_e \tag{12}$$

$$u_{fc} = (2\ (p_e - p_c)/\rho_f)^{1/2} \tag{13}$$

$$\rho_{gc} = p_c / R\ T_{gc} \tag{14}$$

$$T_{gc} = T_e\ (p_c/p_e)^{(k-1)/k} \tag{15}$$

$$u_{gc} = (2\ C_{pg}\ (T_e - T_{gc}))^{1/2} \tag{16}$$

where the kinetic energy of the flow entering the orifice has been neglected. The void fraction of the flow is given by

$$\alpha = \rho_f\ u_f\ x_e / (\rho_g\ u_g\ (1-x_e) + \rho_f\ u_f\ x_e) \tag{17}$$

where the mass quality is x_e since the dissolved gas content of the liquid is assumed to be frozen in the orifice. The mass flow rate of the downstream orifice is then given by

$$\dot{m}/A_c = C_{fc}\ (\alpha\ \rho_g\ u_g + (1-\alpha)\ \rho_f\ u_f)_c \tag{18}$$

where the flow coefficient appearing in the RHS of Eq. (18) is the only empirical parameter in the analysis. This flow coefficient was determined empirically, since it is likely to depend on the specific geometry of the injector orifice. Given the temperature, pressure, and mass quality in the expansion chamber, and the ambient pressure,

Eqs. (10)-(18) provide all properties at the exit of the injector, as well as the overall mass flow rate.

A sketch of the locally homogeneous flow model of the injector orifice appears in Fig. 14. The locally homogeneous flow approximation is most realistic for a bubbly flow, since this configuration maximizes the interfacial area available for interphase transport; therefore, this case is illustrated in Fig. 14. The results of Section 2.3.1 indicated that bubbly flow is also plausible for present test conditions. The other major assumptions are typical of locally homogeneous flow models [15], as follows:

i. The flow is steady and one-dimensional, i.e., all properties are uniform over each cross section of the flow.

ii. The exchange of heat, mass and momentum between the phases is infinitely fast; therefore, both phases have the same velocity, temperature and pressure at each point in the flow.

iii. Wall friction is negligible.

iv. Thermodynamic equilibrium is maintained, i.e., dissolved gas continues to come out of solution as the pressure decreases.

v. Thermodynamic properties of the saturated dissolved gas mixture are obtained from the Soave equation of state as described in Ref. 1.

v. The flow is adiabatic and frictionless (isentropic).

In this case, the flow is also subject to choking at sufficiently high pressure ratios--which is the situation illustrated in Fig. 14. The choked flow condition was determined by computing the mass velocity as a function of back pressure for given inlet conditions. The mass velocity reaches a maximum at a particular value of the back pressure, which defines the orifice exit conditions for choked flow in a convergent nozzle. At higher back pressures than the choked flow condition, the back pressure and orifice exit pressure are the same--similar to one-dimensional compressible flow.

The computation of enthalpy, mass quality, temperature and density as a function of pressure for an isentropic expansion of a saturated dissolved gas system is fully described in Ref. 1. Given properties at the inlet and exit of the orifice, the fluid velocity at the exit and the mass flow rate are found from

$$u_c = (2\ (h_e - h_c))^{1/2} \tag{19}$$

$$\dot{m}/A_c = C_{fc}\ (\rho u)_c \tag{20}$$

Similar to the separated flow model, C_{fc} is the only empirical parameter in the formulation.

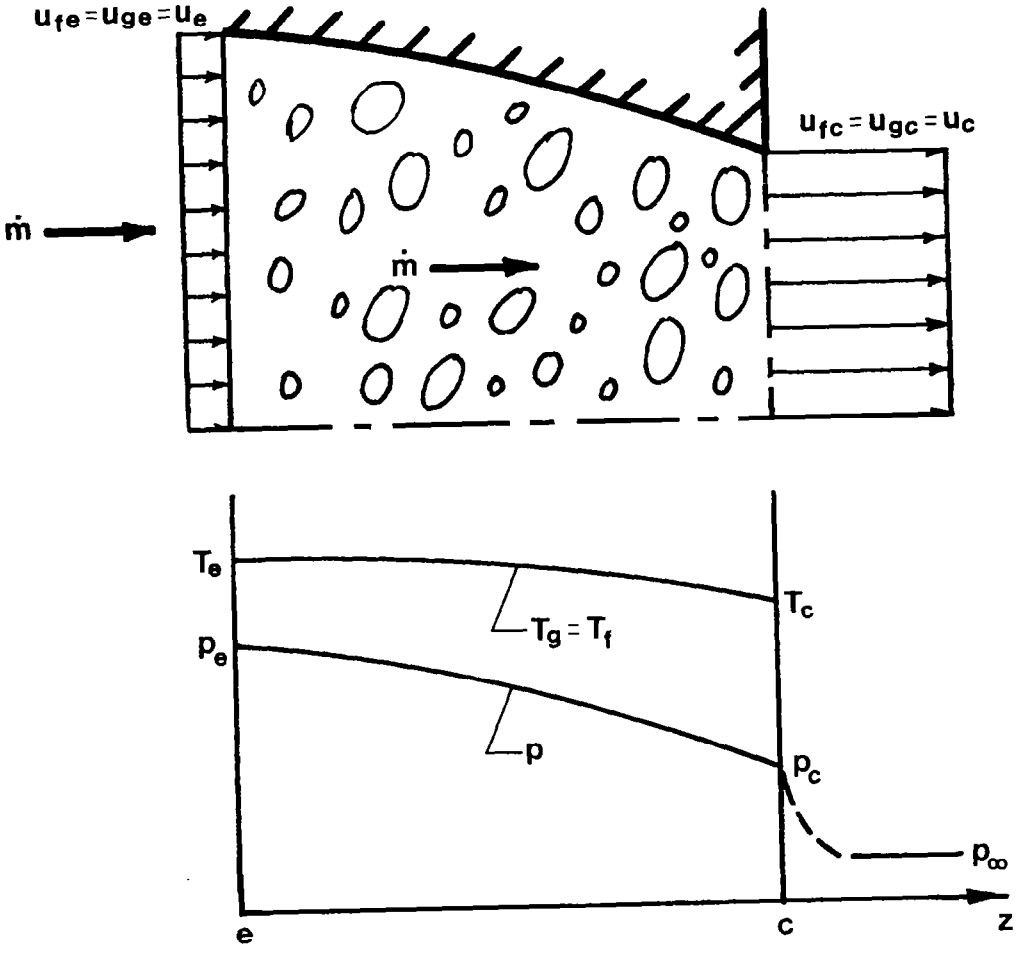

Figure 14. Sketch of the locally homogeneous flow model of the injector orifice.

2.3.3 SMD Correlations

The present investigation involved injection of neat nonflashing liquid, flashing liquids containing dissolved gases, and neat flashing liquids. Correlation of SMD measurements was limited to the first two cases, since subsequent evaporation of neat flashing liquids after injection makes SMD measurements questionable in this case. Expressions for correlating SMD data were obtained by adapting existing results in the literature.

Numerous correlations of SMD for liquid jets from constant diameter passages with no swirl have been reported. Adelberg [34], Mayer [35], and Reitz [36] review existing results in this area. At low liquid jet velocities, capillary forces dominate breakup and Rayleigh has shown that drop sizes are comparable to injector diameters [34]. Present test conditions involved significant aerodynamic effects, however, due to the relatively high velocity of the liquid. Mayer [35] develops an expression for SMD when aerodynamic breakup effects are important as follows [34]

$$SMD = 21.4B \left[\frac{\mu_f (\sigma_f/\rho_f)^{1/2}}{\rho_g u_f^2} \right]^{2/3} \tag{21}$$

where B is an empirical parameter of order unity.

Adelberg [34] extends this approach for estimating drop sizes for liquid jets by subdividing the aerodynamic breakup regime into a capillary wave region (not to be confused with the low velocity capillary breakup regime of Rayleigh) and the acceleration wave region. For the present configuration, the capillary wave regime is defined by

$$(\sigma_f/\rho_g d_p u_f^2)^{1/2} > E \tag{22}$$

where $E \simeq 8 \times 10^{-3}$. In this region

$$SMD = 1.2 B' d_p^{1/2} \left[\frac{\mu_f (\sigma_f/\rho_f)^{1/2}}{\rho_g u_f^2} \right]^{1/3} \tag{23}$$

where B' is a constant of order unity. The flow is in the acceleration wave regime when the inequality of Eq. (22) is not satisfied. In this case, Adelberg finds an expression identical to Eq. (21), except for somewhat different empirical factors. The identification of these flow regimes is not well established at this time; therefore, both Eqs. (21) and (23) were employed during the present investigation.

The velocity of the liquid, appearing in Eqs. (21) and (23) was from

$$u_f = (2\ (p_e - p_\infty)/\rho_f)^{1/2} \tag{24}$$

which implies a velocity coefficient of unity. In view of the other uncertainties in the SMD correlation, this approach is reasonable.

When dissolved gas is present in the liquid, there is a two-phase flow in the injector orifice. For present purposes, this flow was viewed as a separated flow, corresponding to the model illustrated in Fig. 13. This flow configuration is similar to a prefilming type air blast injector, since the liquid is spread along the surface of the injector passage as an annular film. Lefebvre [8] has recently reviewed methods for correlating SMD from injectors of this type. The formula chosen for the present study has the following (dimensional) form,

$$\eta_n SMD = 0.073 \left(\frac{\sigma_f}{\rho_g\ u_g^2}\right)^{0.6} \left(\frac{\rho_f}{\rho_g}\right)^{0.1} d_p^{0.4} \left(1 + \frac{\dot{m}_f}{\dot{m}_g}\right)$$

$$+ 0.0006 \left(\frac{\mu_f^2\ d_p}{\sigma_f\ \rho_g}\right)^{0.5} \left(1 + \frac{\dot{m}_f}{\dot{m}_g}\right) \tag{25}$$

where all units are in the SI system (m, N, s, kg). The prefilmer lip diameter, d_p, was taken to be the injector diameter while the gas velocity was obtained from Eqs. (10)-(16) during the present study. The factor η_n is an atomization efficiency based on the performance of a particular injector [8] --this parameter was determined empirically during the present study. For conditions of the present tests, the first term on the RHS of Eq. (25) dominates the determination of SMD.

2.4 Results

The atomization tests involved measurements with Jet A fuel containing various amounts of dissolved gas (fixed by the saturation pressure of the air in the fuel tank) as well as superheated Freon 11. The properties of the test fluids considered during the present investigation are summarized in Table 2.

The various injector configurations illustrated in Fig. 6 were examined throughout the investigation. Variation of the expansion volume for the test range was found to have no influence on injector mass flow rates, SMD or spray angles; therefore, in the following all results pertain to configuration A.

Table 2 Summary of Atomization Test Conditions[a]

Fluid	Supply Conditions		
	Pressure (MPa)	Temperature (K)	Mole Fraction of Dissolved Air
Jet A	3.45	298	0.050
Jet A	6.87	298	0.100
Jet A	10.34	298	0.151
Freon 11	1.73	370	0

[a]Injector orifice was a straight-hole passage, 0.2 mm diameter, 0.4 mm long (Spraying Systems Co. Model 000009, Solid Stream Tip).

The data obtained during this portion of the investigation are summarized in the Appendix.

2.4.1 Injector Flow Rates

The first phase of the measurements involved testing model predictions for injector flow rate as a function of dissolved gas content and expansion chamber conditions. The upstream orifice, where flashing effects are small, and the injector orifice, which involves a two-phase flow, were considered separately.

The various orifices used in the universal injector are relatively small; therefore, flow coefficients were measured for all of them. The flow coefficient measurements are summarized in Table 3.

The upstream orifices were only calibrated for liquid flow. The flow coefficients listed for them in Table 3 are relatively small due to the small size of the orifices and the difficulty in accurately determining their minimum diameter. The flow coefficients of the upstream orifices were relatively constant over the range of pressure drops that they experience during injector operation.

The injector orifice was calibrated for several types of flow. This included Jet A containing no dissolved air, air flow alone and two-phase flows for the limiting cases of locally homogeneous and separated flow. In cases where gases were present, the models described in Section 2.3.2 were employed to provide the ideal flow estimate--allowing for compressibility.

It was possible to find a single flow coefficient in each case which correlated the complete range of the data. When the two-phase models were considered, these flow coefficients also provided an empirical correction for fundamental deficiencies in each model, e.g., the actual flow involves some slip between the phases and some entrainment of liquid and gas so that neither model completely corresponds to the actual flow condition. Therefore, it is not surprising that the flow coefficient for the locally homogeneous model slightly exceeds unity. In view of the difficulty in accurately measuring the diameter of the injector orifice, it is encouraging that the two-phase flow coefficients in Table 3 are all reasonably close to unity.

Predicted and measured mass flow rates through the upstream orifice are illustrated in Fig. 15. The measurements are for Jet A saturated with dissolved air at the upstream pressure--considering two different saturation pressures. Various upstream orifices were used to cover the range shown in the figure. The measured flow rates are normalized by the flow coefficient given in Table 3 for neat liquid. The theoretical mass flow rates were obtained from Eq. (7)--which assumes that no flashing occurs in this orifice. The results with dissolved air present are seen to be comparable to the findings for neat liquid, suggesting that flashing is not of major importance in the upstream orifice for present test conditions.

Table 3 Summary of Orifice Flow Coefficients

	Diameter (mm)	Flow Coefficient
Upstream Orifice:[a]		
Jet A	0.46	0.85
Jet A	0.33	0.75
Jet A	0.25	0.88
Jet A	0.20	0.84
Jet A	0.15	0.72
Jet A	0.10	0.65
Jet A	0.076	0.77
Injector Orifice (single-phase flow):[a]		
Jet A	0.20	0.66
Air	0.20	0.90
Injector Orifice (separated flow):		
Jet A/Air	0.20	0.91
Freon 11	0.20	0.88
Injector Orifice (locally homogeneous flow):		
Jet A/Air	0.20	1.15
Freon 11	0.20	0.94

[a]Evaluated for pressure drops in the range 1.7-10.3 MPa. Standard deviation of flow coefficient was 0.03 over this range.

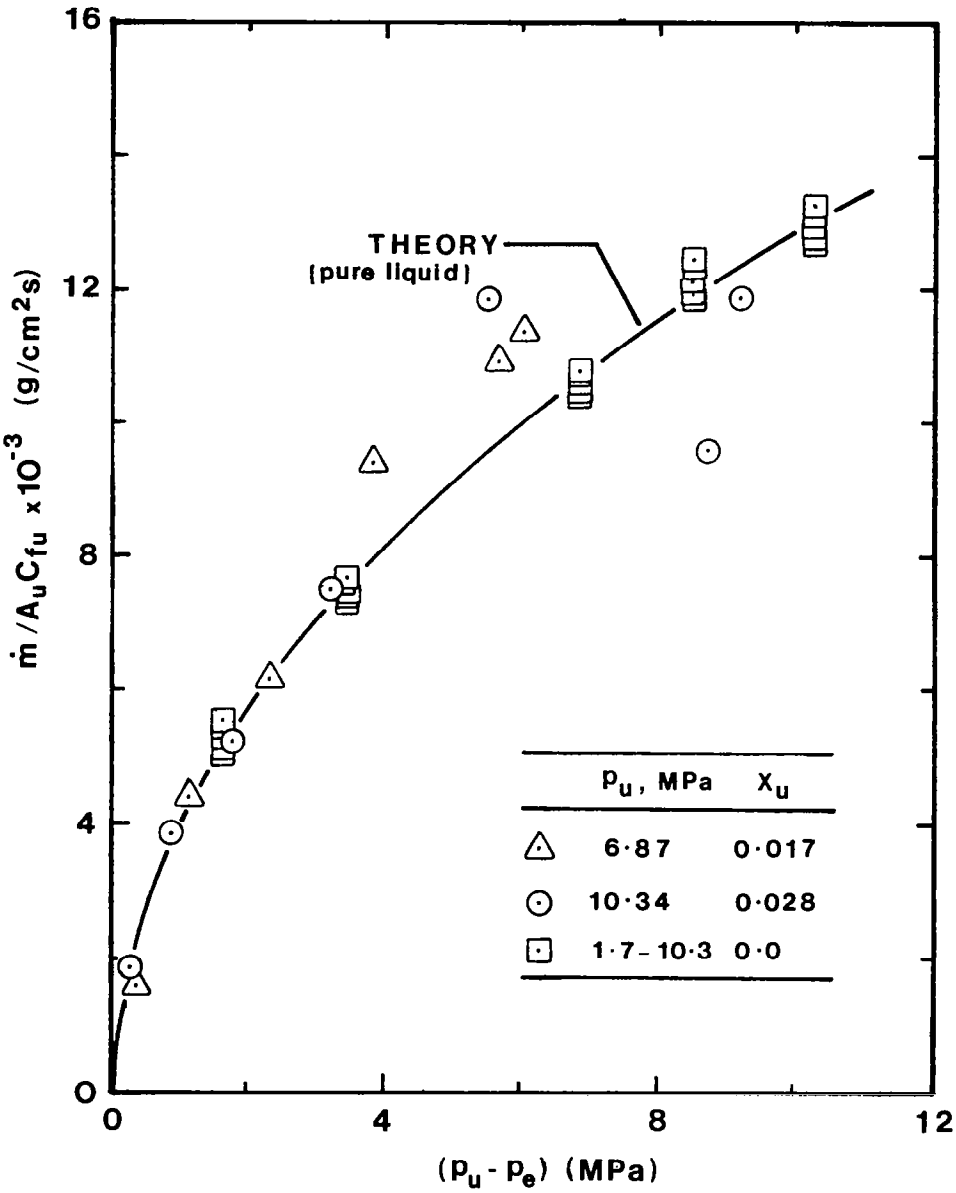

Figure 15. Upstream orifice mass flow rates for Jet A containing dissolved air.

The two-phase flow properties of the injector orifice were predicted using the method of Chisholm [32] as well as the separated and locally homogeneous flow models described in Section 2.3.2. As noted earlier, the Chisholm method was not satisfactory since it does not account for compressibility effects which were important for present test conditions; therefore, this approach will not be considered here.

The mass flow rate predictions of the separated and locally homogeneous flow models are compared with the measurements in Fig. 16. Also shown on the plot is the prediction for a flow of neat liquid, using Eq. (7) and the liquid flow coefficient in Table 3 for this orifice. The tests include three dissolved gas levels (represented by the saturation pressure) and values of p_e/p_∞ in the range 0-100.

Flashing of dissolved air in the expansion chamber is seen in Fig. 16 to reduce the maximum mass velocities attainable in the injector orifice. The effect is due to the reduced density of the flow as a result of the presence of gas. This implies that larger injector passage diameters are needed to pass a given flow rate of fuel for flashing injectors. The larger passage size is a potential benefit since the danger of clogging is reduced, although this effect is not very large for present test conditions. This advantage for the flashing injector concept was originally anticipated by Marek and Cooper [2].

The results of Fig. 16 show that increasing the concentration of dissolved gas causes a progressive reduction in the mass flow rate of the injector orifice for a given pressure ratio. The locally homogeneous flow model predictions provide the best indication of these trends--and are also in good quantitative agreement with the measurements upon selection of a single empirical flow coefficient. The separated flow model also provides a fair prediction of the measurements--and has the advantage of being relatively easy to use since it does not require consideration of relatively complex high pressure equations of state for dissolved gas systems.

The flow properties of the upstream orifice for flashing Freon 11 are illustrated in Fig. 17. In addition to the measurements, predictions for pure liquid and locally homogeneous flow of flashing liquid are also shown (since flashing does not occur upstream of this orifice, the separated flow model cannot be applied). The results indicate that effects of flashing are negligible in this orifice, similar to the Jet A/air system.

The flow properties of the injector orifice for flashing Freon 11 are illustrated in Fig. 18. As before, flashing in the expansion chamber reduces the mass flow rate from the value that is predicted for pure liquid. Similar to the Jet A/dissolved gas system, the locally homogeneous flow model provides the best flow rate predictions. The predictions for the separated flow model are also acceptable, however, in this case both models have similar computation requirements and there is little advantage for the separated flow model.

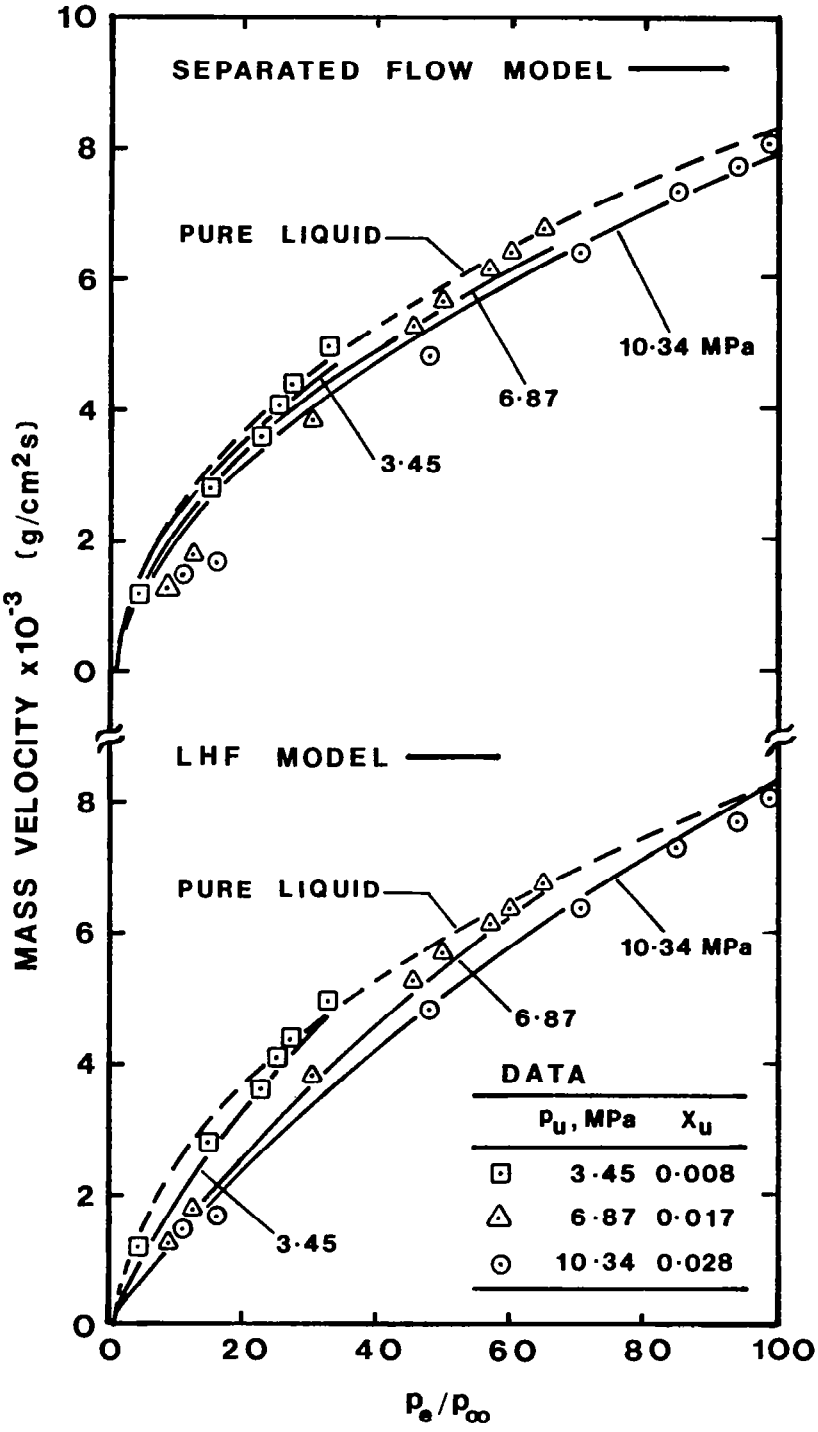

Figure 16. Injector orifice mass flow rates for Jet A containing dissolved air.

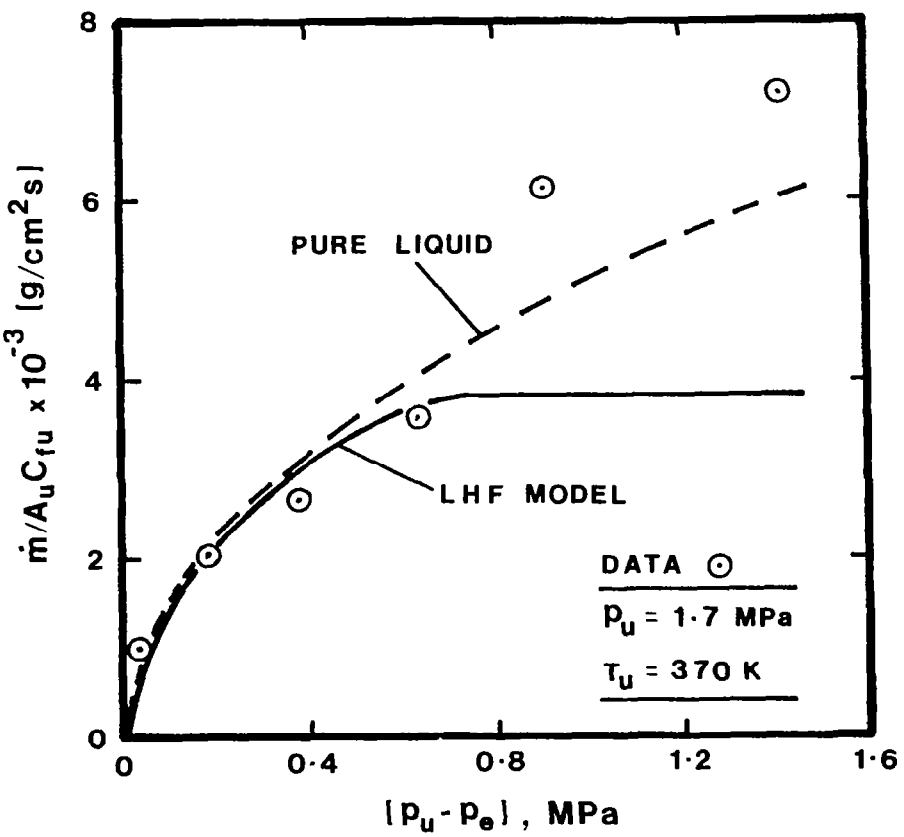

Figure 17. Upstream orifice mass flow rate for superheated Freon 11.

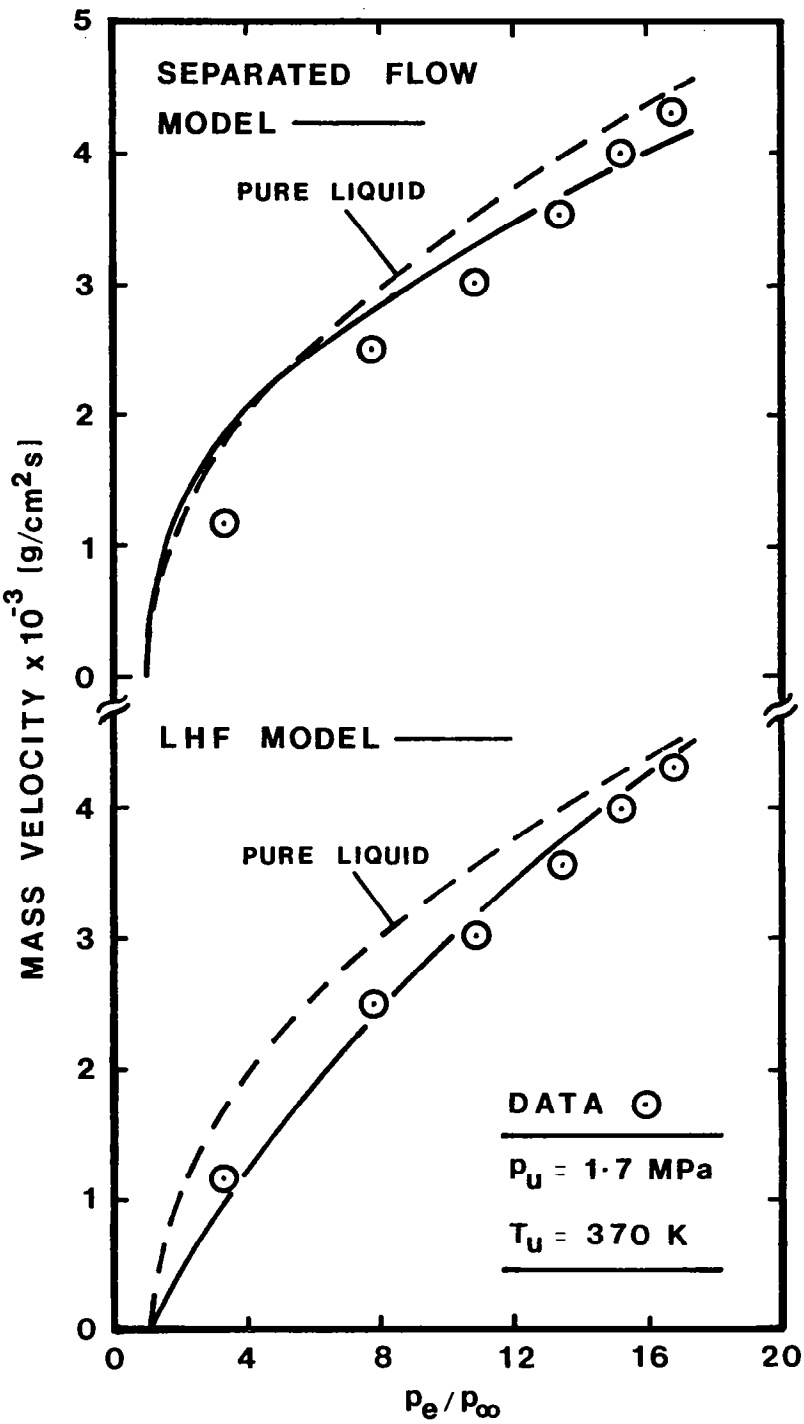

Figure 18. Injector orifice mass flow rate for superheated Freon 11.

2.4.2 Spray SMD

Typical drop size distributions for injection of Jet A are illustrated in Figs. 19-22. Figures 19 and 20 are for no dissolved gas while Figs. 21 and 22 are for dissolved gas mass fractions of 0.028. The injector orifice pressures of Figs. 19 and 21, and 20 and 22 are comparable; therefore, comparing these figures gives an indication of the effect of dissolved gas on drop size distribution. Of the four conditions shown, the case where the gas is partially flashed in the expansion chamber, Fig. 22, yields the highest percentage of small drops.

The data shown in Figs. 19-22 is the weight-averaged distribution obtained from the Malvern instrument using the model-independent analysis. This information was processed to obtain the SMD as follows

$$SMD = \sum_{i=1}^{N} w_i / \left(\sum_{i=1}^{N} w_i / d_i \right) \qquad (26)$$

where N is the number of drop size groups and w_i is the weight fraction of drops in group i--which has a mean diameter d_i, cf. Table 4.

The SMD for all the injector conditions varied with both axial and radial position in the spray, similar to Fig. 11. The present measurements were limited to the centerline of the flow. This was sufficient since the main objective of the measurements was to determine whether the flashing injector concept improved atomization. Furthermore, SMD measurements were not undertaken with Freon 11, since this fluid is very volatile and drop evaporation strongly influences the results. In contrast, Jet A is a relatively non-volatile fuel so that drop evaporation is negligible for the portion of the spray that was considered [11].

The variation of SMD with axial distance from the injector, for Jet A containing no dissolved air, is illustrated in Fig 23 for three different injector orifice pressure ratios. In general, SMD reaches a minimum near the injector and then gradually increases with increasing distance from the injector. These trends are due to several flow phenomena of the spray as well as limitations of the Malvern drop size instrument near the injector. Drop sizes tend to decrease near the injector due to secondary breakup, since drops have the largest relative velocities in this region tending to exceed Weber numbers needed for breakup. The spray is relatively dense near the injector as well, which results in excessive obscuration of the laser beam used by the Malvern instrument, so that significant secondary scattering of light occurs. When secondary scattering is important, the analysis of the light distribution at the detector in order to determine SMD begins to break down and the indicated SMD is no longer reliable; therefore, the trend of decreasing SMD near the injector may be due to instrument errors, even though secondary breakup could explain the results.

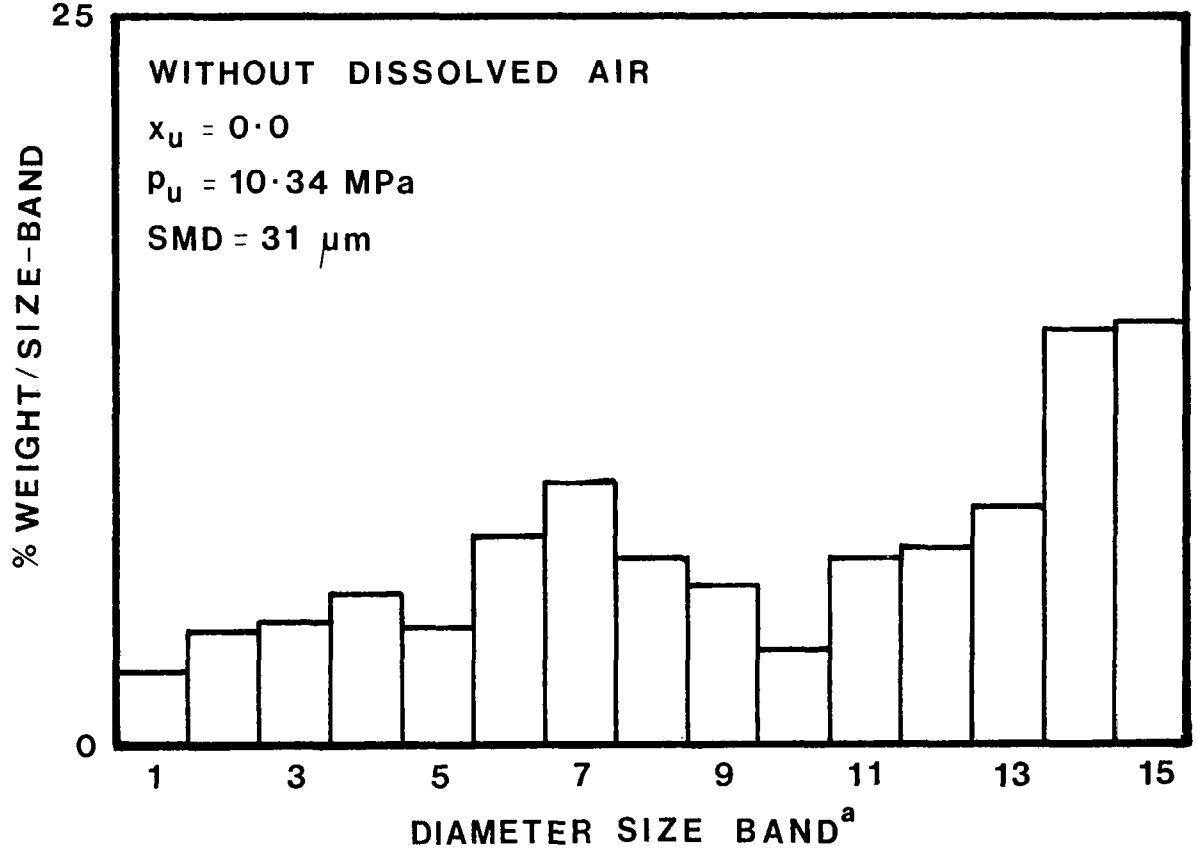

Figure 19. Drop size distribution for Jet A containing no dissolved air for an injector orifice inlet pressure of 10.34 MPa. Size range for groups 1-15 is 6-564 μm.

[a]See Table 4 for lower and upper limits of size bands.

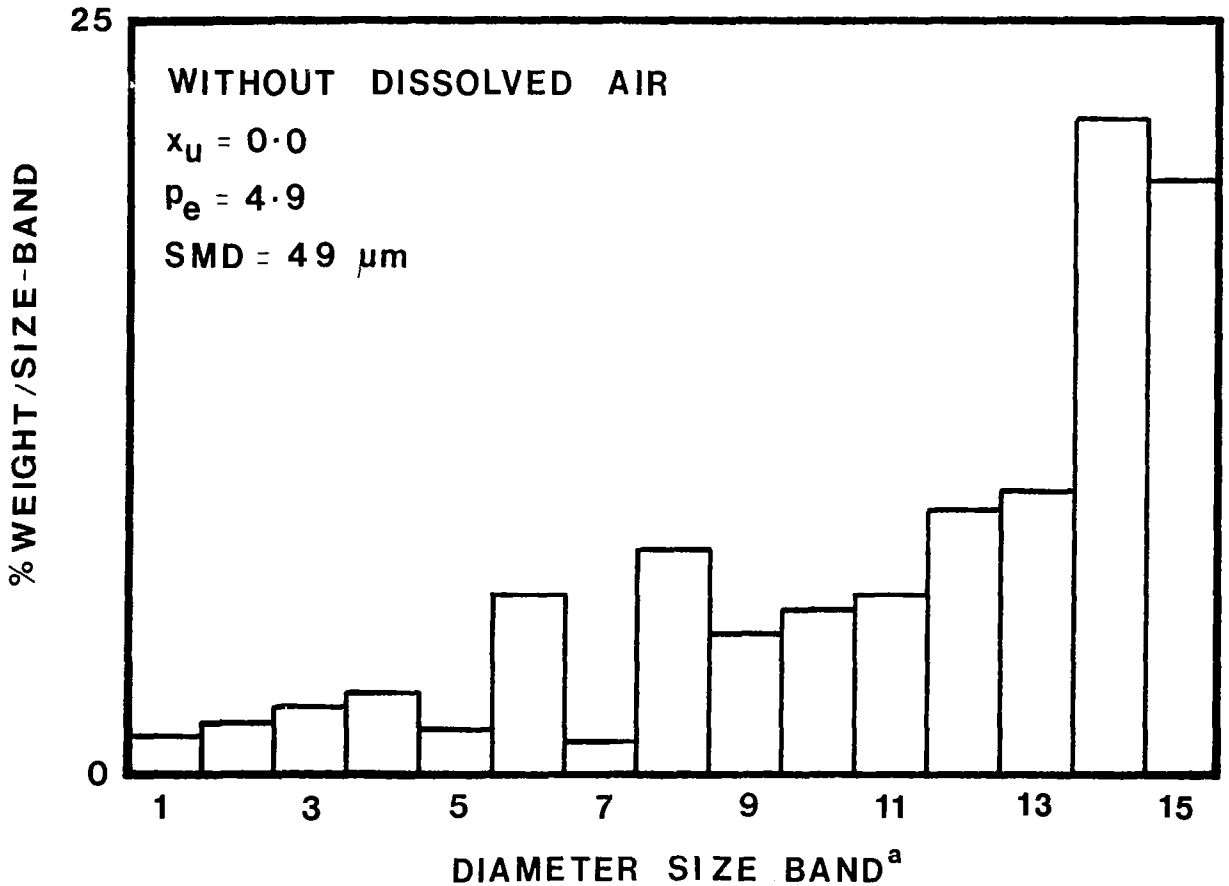

Figure 20. Drop size distribution for Jet A containing no dissolved air for an injector orifice inlet pressure of 4.9 MPa. Size range for groups 1-15 is 6-564 μm.

[a]See Table 4 for lower and upper limits of size bands.

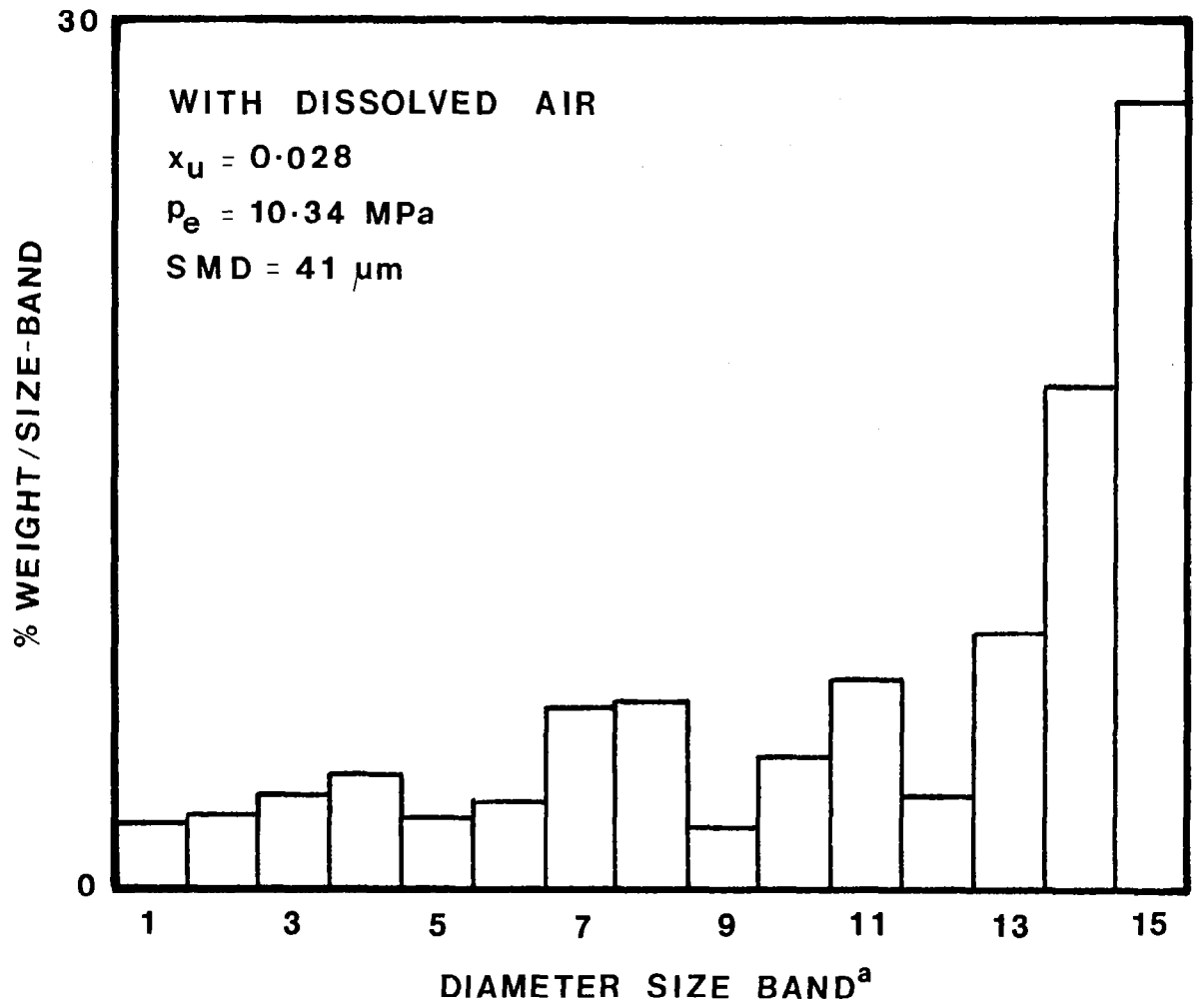

Figure 21. Drop size distribution for Jet A containing dissolved air with negligible pressure drop in the upstream orifice and an injector inlet pressure of 10.34 MPa. Size range for groups 1-15 is 6-564 μm.

[a]See Table 4 for lower and upper limits of size bands.

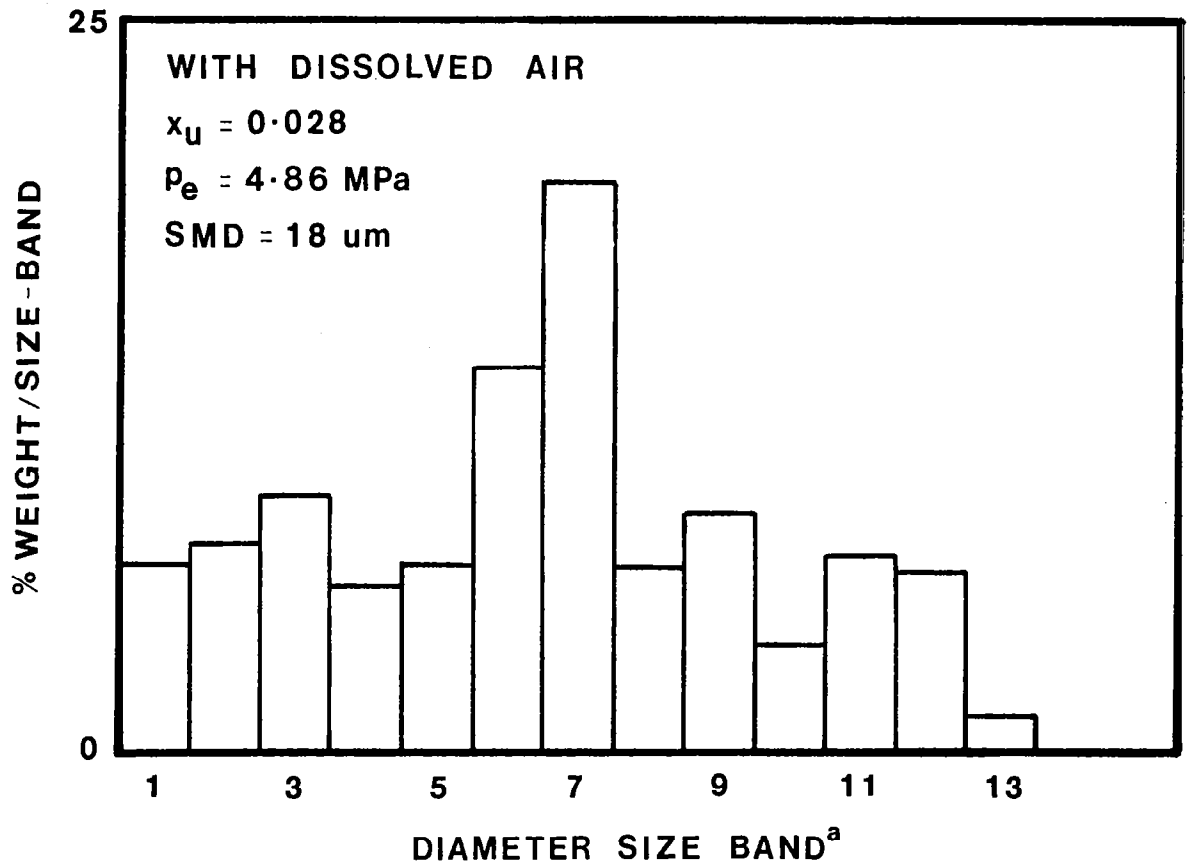

Figure 22. Drop size distribution for Jet A containing dissolved air with an injector inlet pressure of 10.34 MPa and an expansion chamber pressure of 4.86 MPa. Size range for groups 1-13 is 6-160 μm.

[a]See Table 4 for lower and upper limits of size bands.

Table 4. Diameter Size Bands Used to Characterize Drop Size Distribution

Size Band Index	Size Band Range[a] (μm) lower	upper
1	6	7
2	7	9
3	9	11
4	11	15
5	15	19
6	19	24
7	24	30
8	30	39
9	39	50
10	50	65
11	65	84
12	84	113
13	113	160
14	160	260
15	260	564

[a]Mean diameter d_i used in Eq. (26) is the arithmetic mean of the lower and upper limits of each size band.

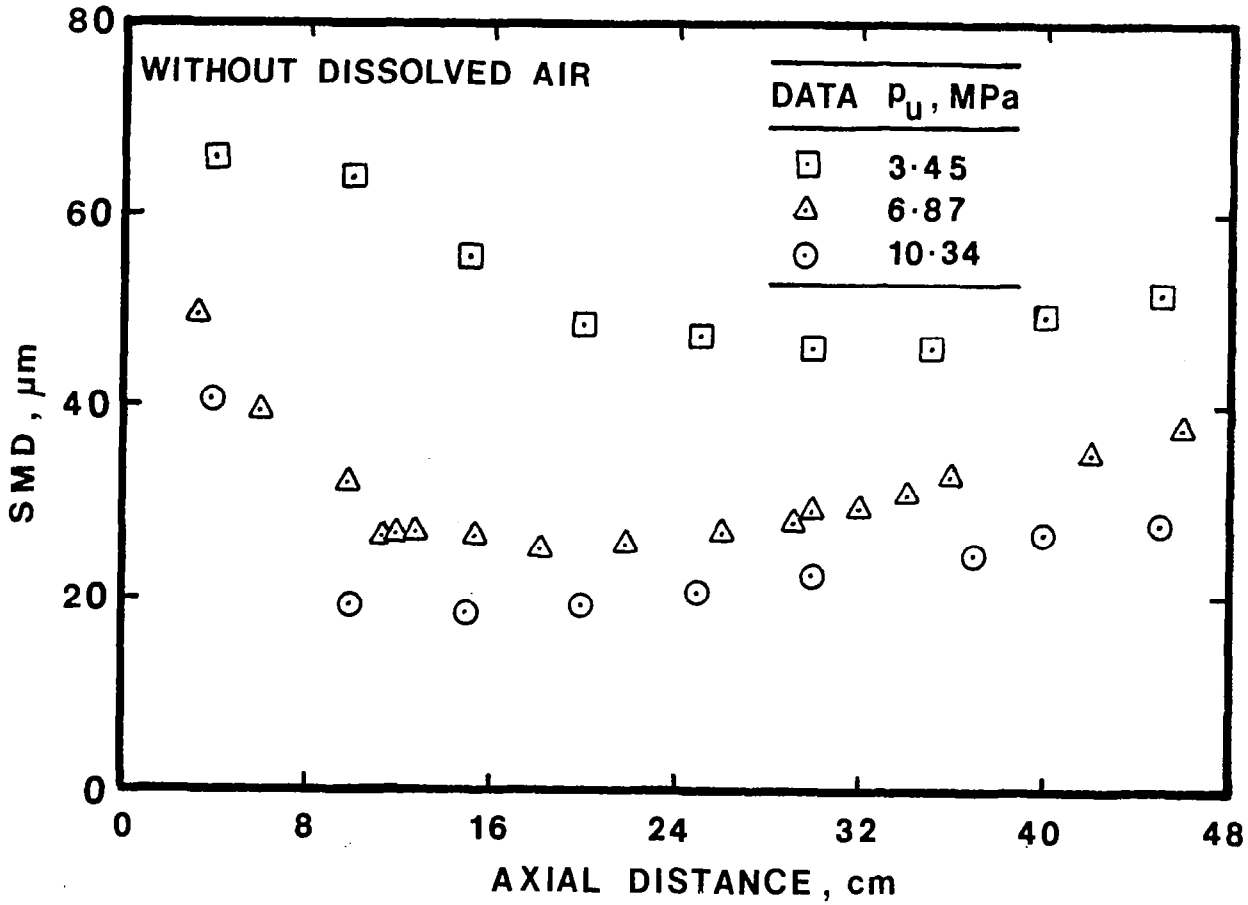

Figure 23. Variation of SMD with axial position for injection of Jet A containing no dissolved air.

At greater distances from the injector the Malvern is operating with limited secondary scattering so that its results are reliable, however, the flow properties of the spray result in changes of SMD along the spray centerline. Three effects can contribute to this behavior--drop evaporation, drop collisions and drop dispersion. As noted earlier, drop evaporation is not important for injection of Jet A into room temperature air; therefore, this phenomena can be ignored for the present measurements. However, O'Rourke and Bracco [37] have shown that drop collisions are very important near straight-hole orifices, which tends to increase the SMD with increasing axial distance from the injector. The effect of drop dispersion causes small drops to spread more rapidly in the flow than large drops--which follow trajectories fixed by injector exit velocities and directions [38]. For a straight-hole injector, this implies that large drops become more concentrated near the centerline at greater distances from the injector. Furthermore, as the Malvern is moved downstream, its laser beam diameter becomes a smaller fraction of the entire width of the spray, also tending to bias the measurements toward the centerline values where the concentration of large drops is greatest.

These general effects were also observed when measurements were made for flashing injection conditions. Figure 24 is an illustration of the variation of SMD with axial position for injection of Jet A containing dissolved gas for a number of operating conditions. The main difference between these results and those for pure Jet A in Fig. 23 is that the minimum of the SMD is reached nearer to the injector. This is due to the fact that sprays from flashing injectors spread more rapidly than nonflashing sprays (this is discussed more fully in the next section) tending to reduce secondary scattering of the Malvern laser beam near the injector and also enhancing the dispersion of small drops [38].

In view of these effects, it is difficult to prescribe an unambiguous SMD for the spray. In order to avoid instrument errors, while reducing the influence of drop collisions and dispersion, a fixed distance from the injector was chosen for the SMD measurements (40 mm from the injector) located near the position where the SMD was a minimum. Measurements at this fixed point at least provide a common basis for comparing injector properties with various degrees of flashing. In view of the effects apparent in Figs. 23 and 24, it is also evident that expressions for spray size, e.g., Eqs. (21)-(25) are only valuable to obtain rough correlations for particular flow and evaporation conditions and distances from the injector.

In the following presentation of SMD variations with operating conditions, the empirical parameters appearing in Eqs. (21)-(25)--B, B' and n_n--were selected to provide a fit of the data at one operating condition. These values are summarized in Table 5.

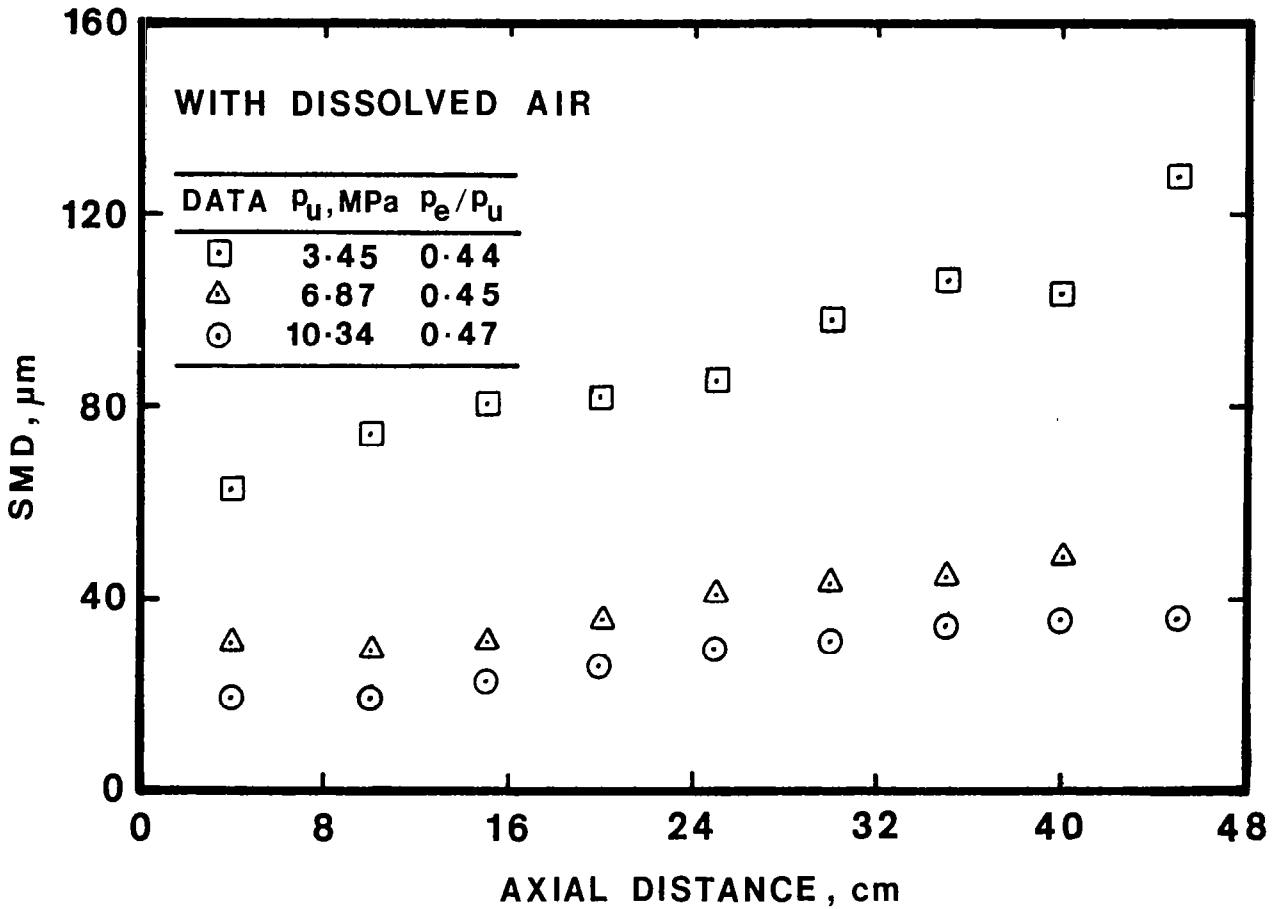

Figure 24. Variation of SMD with axial position for flashing injection of Jet A containing dissolved air.

Table 5 Empirical Parameters Used in SMD Correlations[a]

	B	B'	η_n
Jet A with no dissolved air:	3.0	3.1	--
Jet A/dissolved air:	4.9	5.0	0.35
Correlation equation	Eq. (21)	Eq. (23)	Eq. (25)

[a]Measurement made 40 mm from the injector exit, at the centerline of the spray.

The variation of SMD with injector orifice pressure ratio for Jet A containing no dissolved gas is illustrated in Fig. 25. The measurements were completed for three different pressures at the inlet of the injector; however, only the pressure ratio of the injector orifice has any relevance in this case. The results indicate the expected trend that SMD decreases as injector pressure ratio increases. The predictions of Eqs. (21) and (23), for the acceleration and capillary wave regimes defined by Adelberg [34] are also shown on this plot. The regime boundary estimated from Eq. (22) is beyond the range of the figure. Although the present measurements lie within the capillary wave region defined by Adelberg, the best correlation is achieved using the acceleration wave expression of Eq. (21), (notably, Mayer [35] does not distinguish these regimes and suggests that Eq. (21) is appropriate throughout the aerodynamic breakup region).

The effect of dissolved air on SMD, when an expansion chamber is not used ($p_u = p_e$), is summarized in Table 6. Surprisingly, the presence of dissolved air in Jet A actually results in an increase in the SMD for the three conditions considered in the tests. This finding is similar to that of Sher and Elata [4] who note that little improvement of atomization was obtained when injecting a flashing flow containing dissolved gases unless a flow restriction (which was not defined) was placed upstream of the injector.

A beneficial effect of dissolved air on atomization is achieved when the mixture is allowed to flash in the expansion chamber. Data illustrating this appears in Fig. 26. Measured SMD is plotted as a function of expansion chamber pressure ratio for the three dissolved air concentrations considered in the tests. As the pressure of the expansion chamber is reduced, for a given injector inlet pressure, the SMD decreases, reaching a broad minimum before rising once again at low expansion chamber pressures. Two effects appear to be responsible for this behavior. When the expansion chamber pressure is reduced, more air is flashed and the specific volume of the air increases, tending to provide greater shear between the liquid and gas phases in the injector orifice which results in smaller drop sizes. As the expansion chamber pressure decreases, however, the pressure drop across the injector orifice is reduced, which reduces flow velocities and tends to increase drop sizes. Therefore, the opposing trends of these two effects yield an optimum expansion chamber pressure for given inlet conditions. In contrast, increasing the concentration of dissolved air results in a monotonic decrease in SMD--which is the behavior expected from past investigations of airblast atomizers [8].

The measured SMD values are compared with two correlations in Fig. 26. One is for pure liquid injection, Eq. (21) where the empirical constant has been selected to match injector operation when there is no pressure drop in the expansion chamber. The second correlation employs the airblast atomizer expression of Eq. (25), where η_n has been selected to achieve the best fit of the data. In both cases,

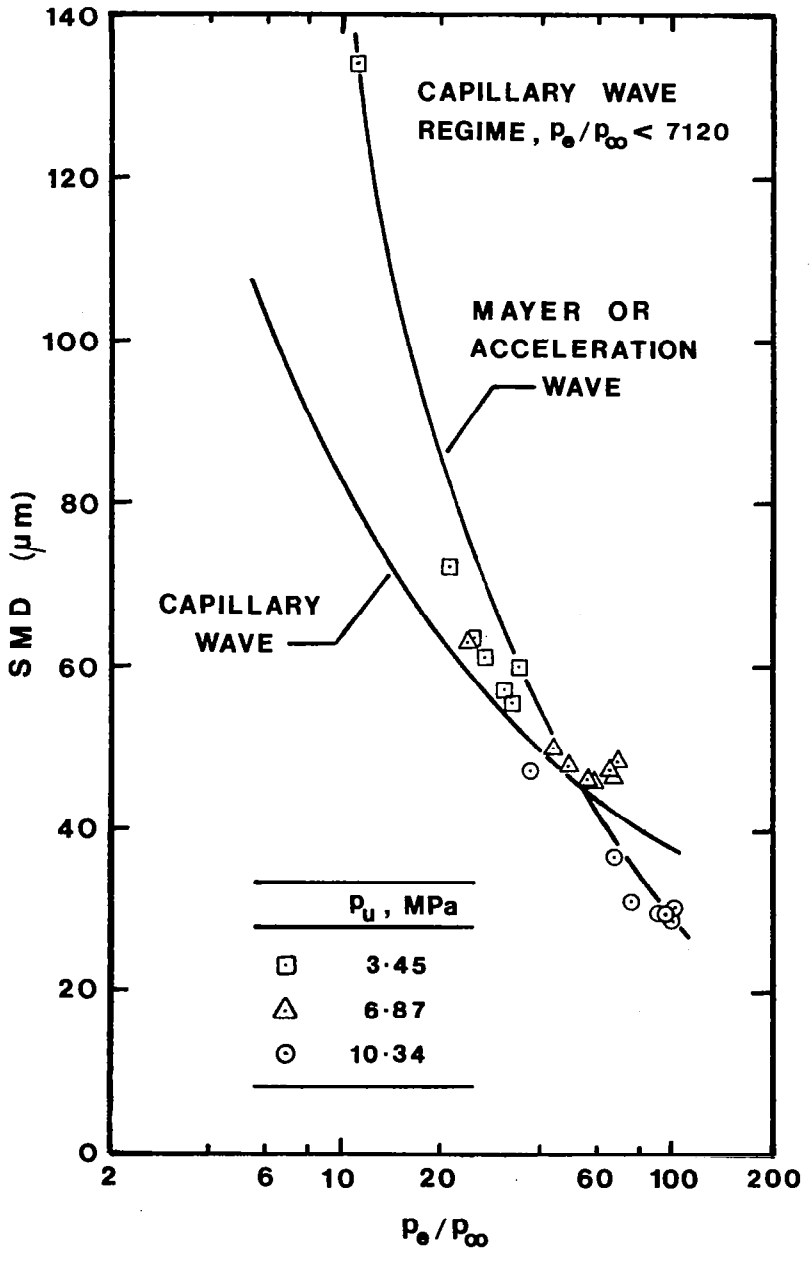

Figure 25. Variation of SMD with injector orifice inlet pressure ratio for injection of Jet A containing no dissolved air.

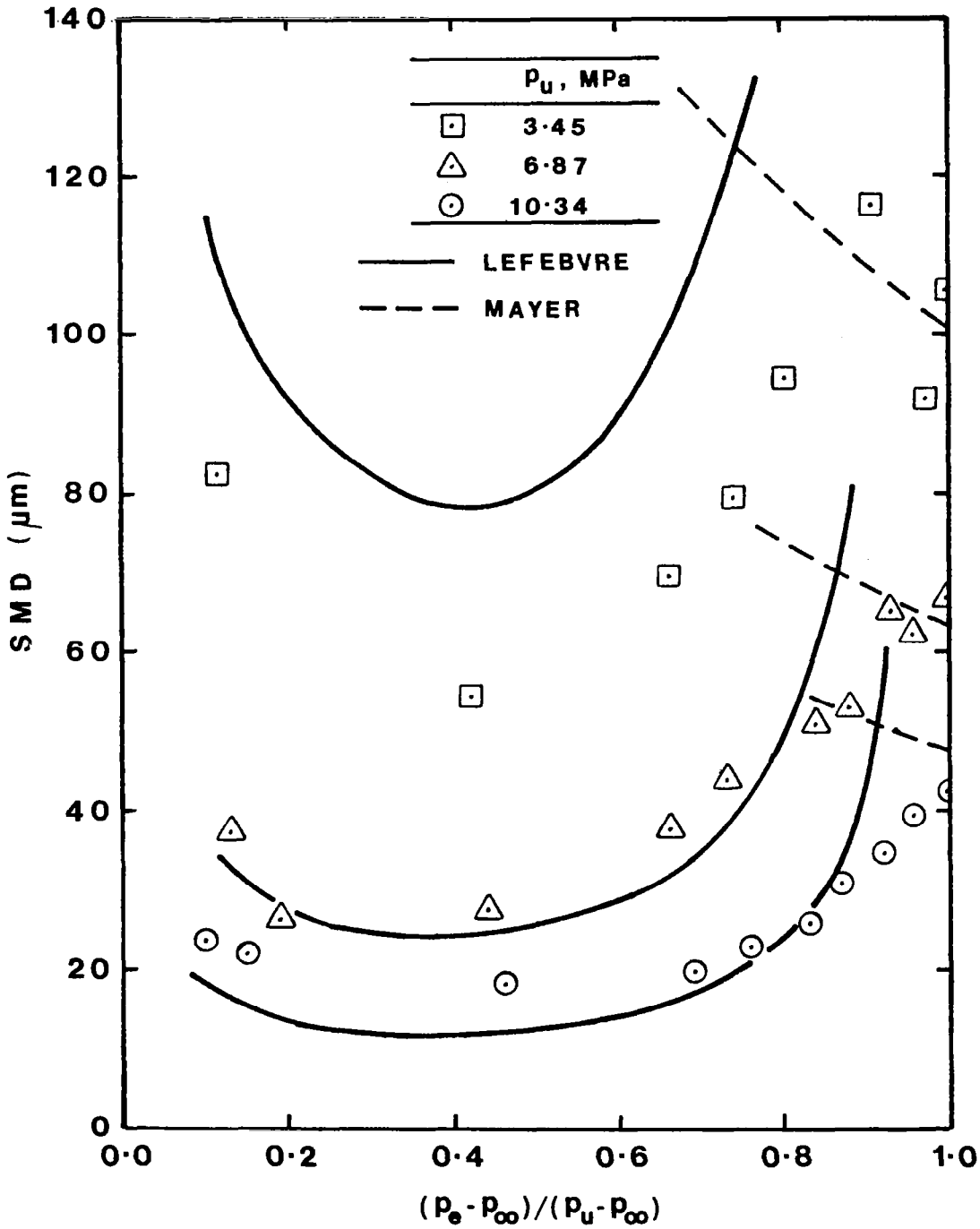

Figure 26. Variation of SMD with expansion chamber pressure for injection of Jet A containing dissolved air.

Table 6 Effect of Dissolved Air on Jet A SMD with No Expansion Chamber

Injector Inlet Pressure (MPa)	Dissolved Air Mass Fraction	SMD (μm)
3.45	0	60
3.45	0.008	106
6.87	0	48
6.87	0.017	66
10.34	0	31
10.34	0.028	43

the magnitudes of the empirical parameters are reasonable. The combined correlations provide a fair representation of the data: Eq. (21) treating the region $p_e \approx p_u$ where the airblast expression breaks down, while the airblast expression provides a fair correlation of the results for low values of expansion chamber pressure. It is also encouraging that the airblast expression provides a reasonable indication of the expansion chamber pressure range where SMD reaches a minimum.

2.4.3 Spray Angles and Liquid Flux Distributions

One of the most dramatic effects of flashing injection of Jet A containing dissolved air was the effect of expansion chamber conditions on the appearance of the spray. Some typical results are illustrated in Fig. 27. Four cases are shown for the same injector inlet pressure: injection of pure liquid with $p_e = p_u$, injection of pure liquid with $p_e = 0.46\ p_u$, injection of Jet A containing dissolved air wtih $p_e = p_u$, and injection of Jet A containing dissolved air with $p_e = 0.47\ p_u$. Only in the last case does flashing occur in the expansion chamber.

It is evident from the photographs in Fig. 27, that the presence of dissolved air has a relatively small effect on the spread of the spray when flashing is not induced in the expansion chamber. The major observable difference between injection of pure Jet A and injection of Jet A containing dissolved gas without internal flashing was that the spray had a more milky appearance and a slightly increased spray angle in the latter case (Table 7 is a summary of the spray angle comparison). The milky appearance suggests that dissolved gas was flashing outside the injector; however, liquid velocities are quite large for these injector pressure ratios (greater than 200 m/s), while bubble growth rates are relatively small for dissolved gas systems (less than 1 m/s). Therefore, while bubble growth yields lateral deflection of the flow, as described by Sher and Elata [4], the effect is small in comparison to the streamwise velocity.

In contrast, when the dissolved gas is flashed in the expansion chamber, the flow is choked in the injector orifice. Therefore, the pressure at the exit of the injector is greater than ambient, yielding an external expansion process similar to choked underexpanded single-phase flows [33]. This yields an increase in spray angle as liquid is deflected in the radial direction due to the expanding gas flow.

The effect of dissolved air content and expansion chamber pressure on spray angle is illustrated in Fig. 28. When $p_e \approx p_u$, the spray angle is not strongly influenced by dissolved gas content. However, as the expansion chamber pressure is reduced, the spray angle increases to a maximum value with the largest spray angles being achieved for the highest dissolved gas concentrations. Similar to the minimum SMD for intermediate expansion chamber pressures, this behavior is due to counteracting effects of two phenomena. As the pressure in the

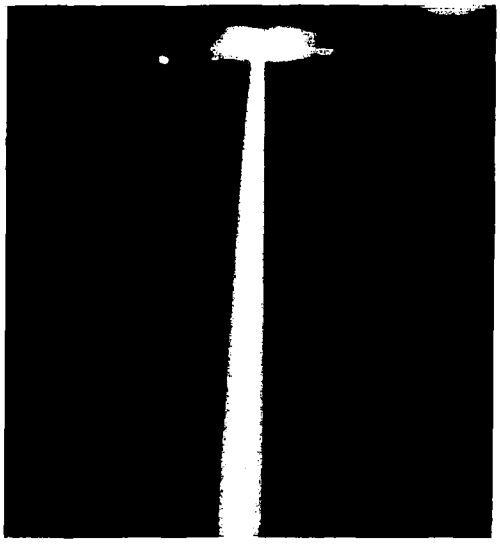

a. Neat liquid, $p_e = p_u$.

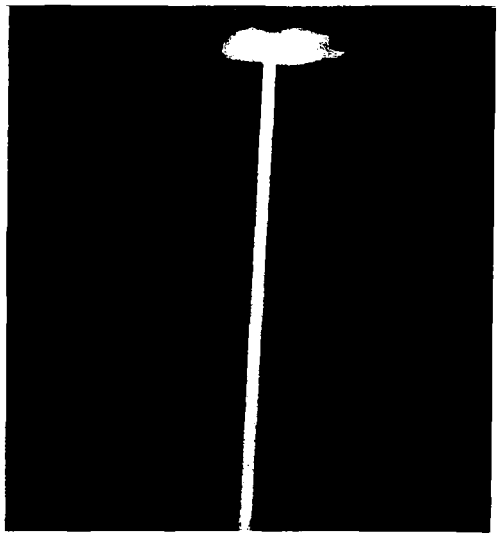

b. Neat liquid, $p_e = 0.46\ p_u$.

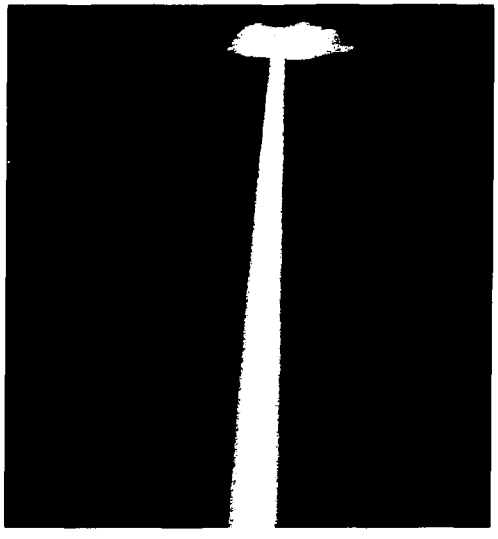

c. Air-saturated liquid, $p_e = p_u$.

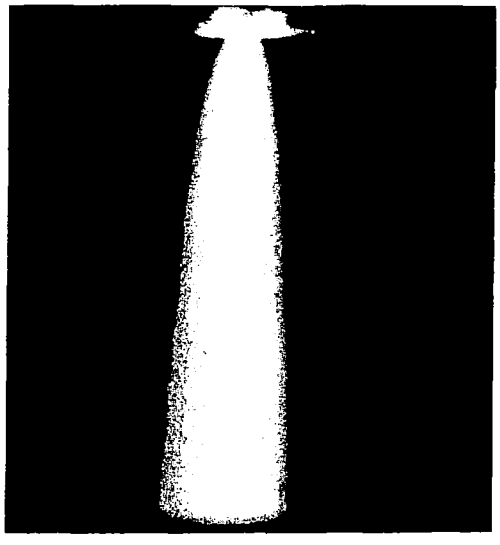

d. Air-saturated liquid, $p_e = 0.47\ p_u$.

Figure 27. Jet A spray appearance, $p_u = 10.34$ MPa.

Table 7 Comparison of Spray Angles for Injection of Jet A with and without Dissolved Gas with No Internal Flashing

Injector Inlet Pressure (MPa)	Dissolved Air Mass Fraction	Spray Angle (^{o})
3.45	0	3.75
3.45	0.008	4.5
6.87	0	4.0
6.87	0.017	5.0
10.34	0	4.0
10.34	0.028	5.0

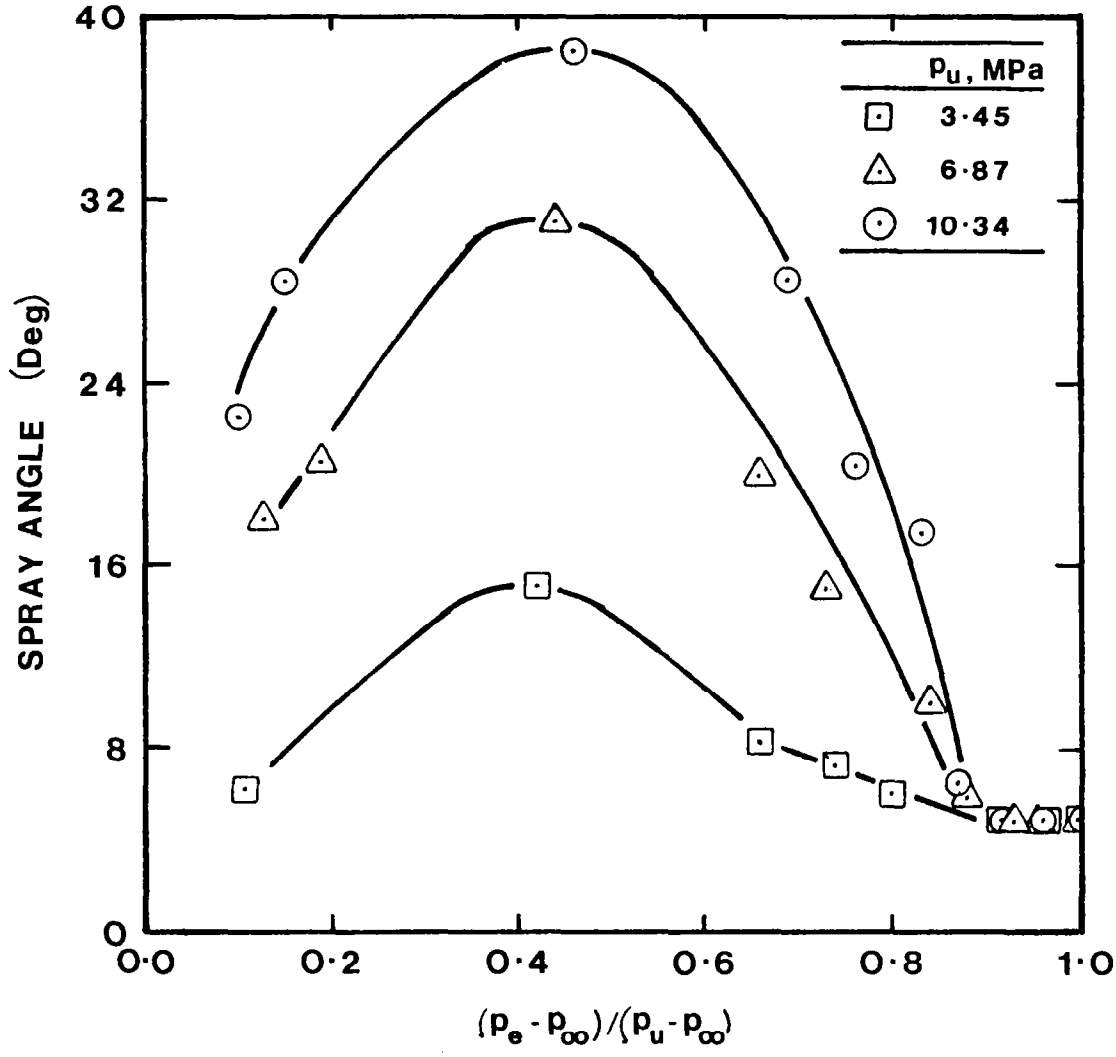

Figure 28. Variation of spray angle with expansion chamber pressure for injection of Jet A containing dissolved air.

expansion chamber is decreased, more air flashes which provides a greater capability for deflecting the liquid flow; however, reduced expansion chamber pressure, lowers the pressure at the exit of the injector which reduces the radial deflection of the gas as it expands to the ambient pressure.

The radial distribution of liquid flux for injection of Jet A with and without dissolved gas present is illustrated in Fig. 29. This data was collected at an axial distance of 530 mm from the injector, for downward injection. As noted earlier, the collection efficiency of the spill-over technique was 70-90% for these conditions since small drops tend to remain entrained with the gas flow and deflect around the opening of the collection tube. The condition illustrated for the Jet A dissolved air system corresponded to the optimum expansion chamber pressure for maximum spray angle and minimum SMD, although the injector inlet pressure was the same for both sets of data. The results indicate relatively symmetric liquid flux distributions for both cases; although, as expected from its larger spray angle, flashing injection yields a wider liquid flux profile. In the case of flashing injection, a full cone spray pattern is maintained--even for the rather large spray angle obtained for this configuration.

Photographs of Freon 11 injection appear in Fig. 30. Three cases are shown for the same injector inlet pressure: no superheating, superheated with no active expansion chamber, $p_e = p_u$ and superheated with $p_e = 0.45\ p_u$. In this case, very poor atomization, with a solid liquid stream leaving the injector, was obtained when the fluid was not superheated. Superheating, however, yielded a relatively large spray angle and reasonably good atomization even when an expansion chamber was not used.

Spray angle measurements for flashing Freon-11 are illustrated in Fig. 31. Spray angle is plotted as a function of expansion chamber pressure for a single superheating condition. As observed earlier in Fig. 30, a relatively large spray angle is obtained even when $p_e \approx p_u$ and there is only a slightly higher optimum spray angle for lower values of p_e. This behavior is different than flashing injection with dissolved gases, since the injector pressure ratio is relatively small, yielding a moderate axial velocity, while bubble growth rates are larger for a pure liquid system. This tends to increase the spray angle in comparison to nonflashing flow--even in the absence of choking effects in the injector orifice. Due to its faster bubble growth rates, the Freon-11 could also be flashing in the injector orifice, even without an expansion chamber, yielding choked flow and external expansion effects; however, the flow rate tests did not provide much evidence for this behavior.

2.5 Discussion

The present tests have shown that flashing even small quantities of dissolved gas (mole fractions less than 15%) can have a significant influence on atomization properties. However, these effects are not very evident unless they are promoted by the use of an expansion chamber in the injector passage. With an expansion chamber at optimum conditions,

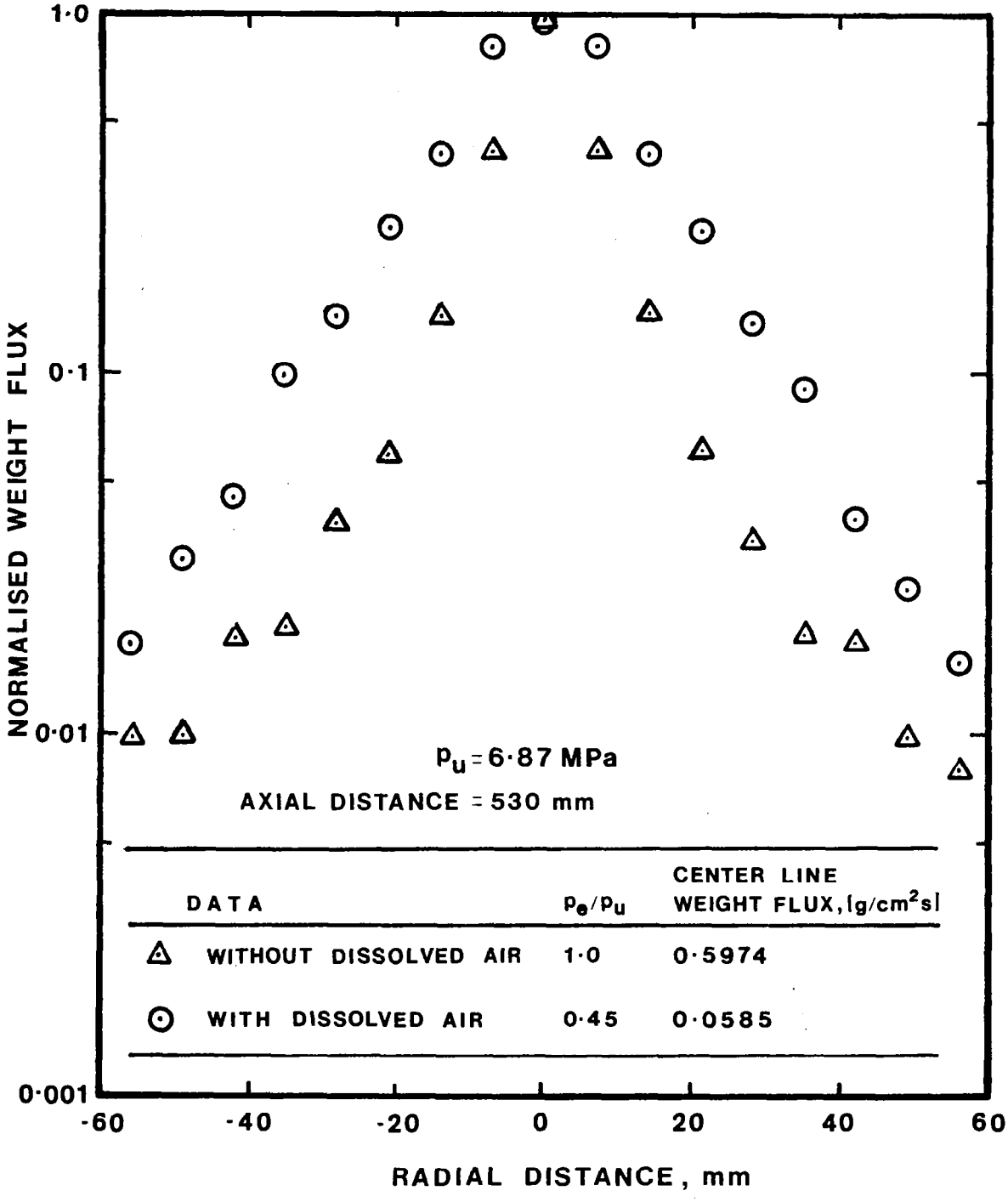

Figure 29. Radial distribution of liquid flux for injection of Jet A with and without dissolved air.

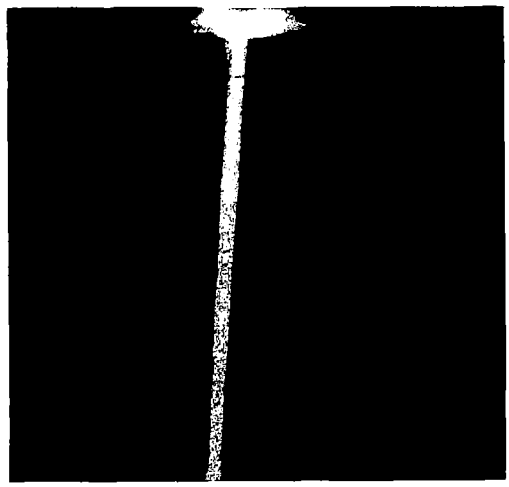

a. No superheating, $p_e = p_u$.

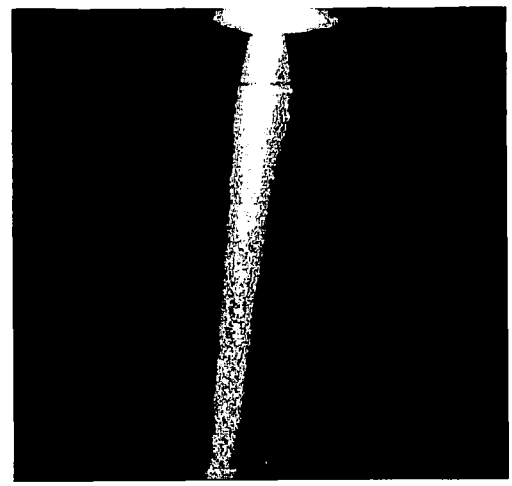

b. Superheated, $p_e = p_u$.

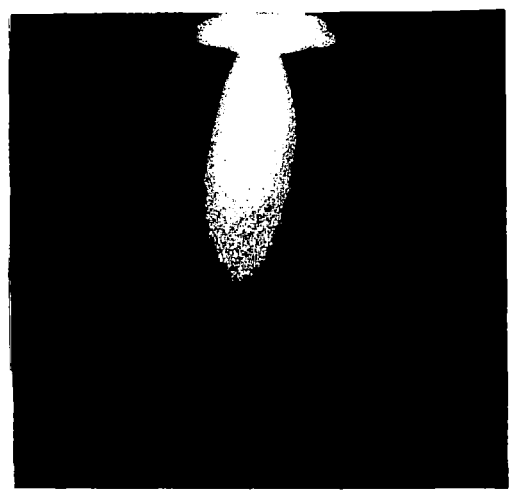

c. Superheated, $p_e = 0.45\ p_u$.

Figure 30. Freon 11 spray appearance, $p_u = 1.7$ MPa.

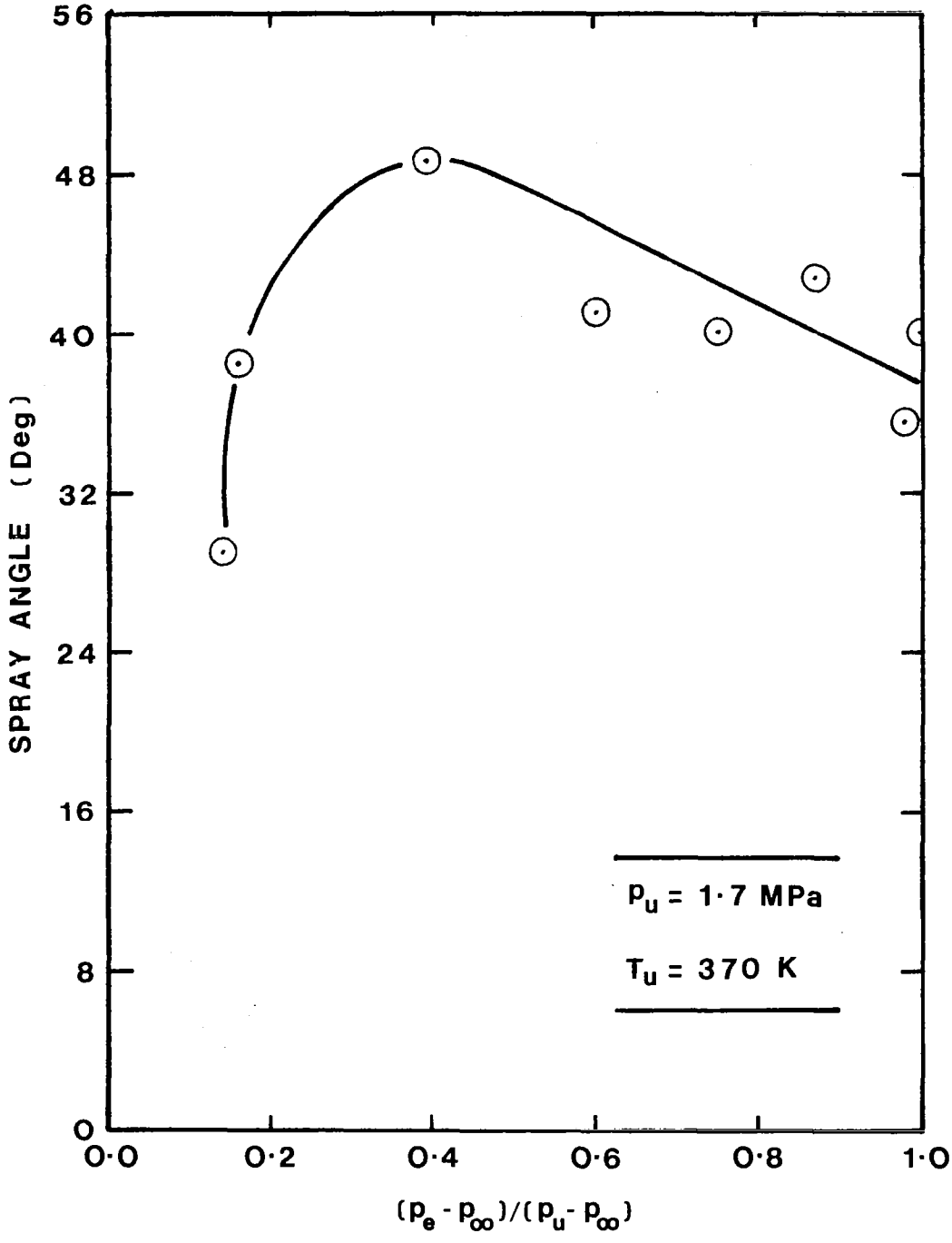

Figure 31. Variation of spray angle with expansion chamber pressure for flashing injection of Freon 11.

larger spray angles and smaller SMD are obtained for Jet A containing dissolved air than is the case for injection of neat fuel, or even fuel containing dissolved air but with no expansion chamber present.

In contrast, a flashing injector operating with a pure superheated liquid achieves larger spray angle, and probably smaller drop sizes, than nonflashing injection even when an expansion chamber is not used. Since the criteria for nucleation are similar in both cases [15], there does not appear to be a question of the presence or absence of bubbles for present test conditions. A more important factor is the relative magnitudes of bubble growth velocities and liquid injection velocities. The present dissolved gas systems required relatively high injection inlet pressures to achieve reasonable dissolved gas concentrations. Furthermore, bubble growth rates are relatively slow for flashing dissolved gas since liquid mass diffusivities are relatively low. Low bubble growth rates and high liquid velocities imply relatively small effects on spray angles and SMD. In contrast, flashing superheated liquids have relatively large bubble growth rates, since bubble growth in this case depends on the thermal diffusivity which is reasonably high for liquids. Furthermore, lower injector velocities were employed for the present flashing liquid tests; therefore, significant effects of flashing on spray angles, and probably drop size, could be observed.

From this discussion, it can be seen that the expansion chamber primarily functions as a means of providing adequate residence time within the injector flow passage for appreciable quantities of dissolved gas to be released from the liquid. Once released, subsequent expansion of the compressible gas provides a means of supplying mechanical energy to the liquid causing increased spray angles and reduced drop sizes. Therefore, an expansion chamber is desirable in those cases where bubble growth rates are small and this is most often the case for dissolved gas systems.

The injector mass flow rate models developed during this investigation provide a reasonably good indication of the flow properties of flashing liquids upon specification of a single empirical flow coefficient. The need for the empirical flow coefficient is not a severe limitation, since flow coefficients must be measured for most injector passages in any event.

The locally homogeneous flow model provided the best estimation of flow properties. This is reasonable, since estimation of flow regimes in the expansion chamber and injector passages suggested bubbly flow for most operating conditions considered here. This flow regime provides the greatest interfacial area between the phases, which makes it easier for equilibrium to be maintained.

The separated flow model also provided a fair estimation of injector flow rates. For dissolved gas systems, in particular, low bubble growth rates imply a more frozen flow in the injector orifices due to their small residence times--which corresponds to the approximations of this model. The separated flow model also is somewhat

easier to use for dissolved gas systems and has the further advantage that it provides parameters for estimating SMD by analogy with airblast injector correlations (in contrast, the locally homogeneous flow model implies no relative velocity between the phases and therefore no airblast effect).

SMD correlations are only rough guides to spray properties since SMD varies appreciably within a spray as a result of secondary atomization, drop collisions, drop dispersion and evaporation. For present test conditions, Eq. (21) due to Mayer [35] and Adelberg [34] provided the best correlation of the effect of injector pressure ratio on SMD of pure liquids and liquids containing dissolved gases but with no expansion chamber present (i.e., small bubble growth velocities in comparison to liquid velocities). Although present tests were within the capillary wave regime defined by Adelberg, Eq. (23), which he proposes for this regime did not provide the best fit of the data.

The general expression of Lefebvre [8] provided a fair correlation of drop sizes when an expansion chamber was used in conjunction with a liquid containing dissolved gas. Application of this formula also required the use of the separated flow model as noted earlier. The nozzle efficiency factor for the present measurements was 35%, which is a reasonable value. This suggests that the downstream injector orifice is behaving somewhat like a prefilming airblast injector. This suggests that procedures used to design airblast injectors can be used to optimize flashing injector performance. Further study is needed to establish whether this is the case, in particular, the effect of downstream orifice size on spray properties should be investigated.

The tests indicated that spray SMD could be minimized and spray angle maximized for particular expansion chamber conditions. The SMD correlation provides a means of determining the optimum condition for minimizing drop sizes; however, a similar expression providing spray angles still must be developed.

The present investigation has not disclosed any particular advantage to dissolving air in the fuel upstream of the injector, since the process of bubble growth in injector passages and near the exit of the injector is relatively slow. Effects that were observed were primarily due to air released from solution in the expansion chamber, which in a sense, operates very similar to the air introduction point of an airblast injector. Conventional use of the airblast injector approach has several advantages over the flashing injector concept. In particular, relative mass flow rates of gas and liquid and the pressure drop across the injector orifice can be freely selected for airblast injectors, to optimize performance, while these parameters are constrained by the thermodynamic properties of the fluid for flashing dissolved gases. In addition, the air need only be pressurized to the pressure upstream of the injector orifice, which is much lower than needed to dissolve appreciable concentrations of air in the fuel.

Based on these observations, the supercritical injector concept [2], should find greatest application when high pressure gas is available in any event, e.g., in gas pressurized fuel feed systems. In this case, the present results indicate that improved atomization properties could be obtained with little effort by allowing the pressurizing gas to dissolve in the liquid and installing an expansion chamber in the injector passage. The widespread use of this approach for household spray cans suggests that the idea is not new and that significant benefits can be achieved in this manner. However, this approach has not been applied to fuel systems and should be given consideration. Another circumstance when these concepts could be applied involves fuels having relatively volatile fractions, where preheating and an expansion chamber could induce flashing injection effects. The flow rate and SMD models developed here should provide assistance to the design of such systems.

3. COMBUSTION STUDY

3.1 Introduction

The atomization study indicated that flashing injection resulted in marked changes in spray properties, e.g., larger spray angles and small SMD, in comparison to conventional injection. The objective of this portion of the investigation was to determine the influence of these changes on the combustion properties of the spray.

Spray configurations for combustor systems vary widely; therefore, an exhaustive investigation of combustion properties was not feasible. During the present investigation a simple arrangement involving an open turbulent spray flame in still air was examined. This configuration has the advantage of being easily specified and reproduced by others. Furthermore, the combustion properties of open spray flames are primarily governed by injection properties--which has been the aspect of flashing injection primarily investigated during this study. Present emphasis was placed on determining the effect of flashing injection on flame shape.

3.2 Apparatus

A sketch of the spray combustion apparatus appears in Fig. 32. The major features of the apparatus are similar to the arrangement used during earlier spray modeling studies in this laboratory [39,40]. The main difference involves modification of the fuel injection system in order to accommodate the flashing injection concept.

The fuel injector was similar to the Universal flashing injector illustrated in Fig. 5. In particular, the injector orifice assembly was the same as Fig. 5; however, the upstream orifice was replaced by a metering valve while the expansion chamber included a 300 mm length of 4.6 mm ID tubing between the metering valve and the injector orifice assembly. As noted earlier, the actual volume of the expansion chamber, at least for sizes greater than configuration C illustrated in Fig. 6, had little effect on atomization properties.

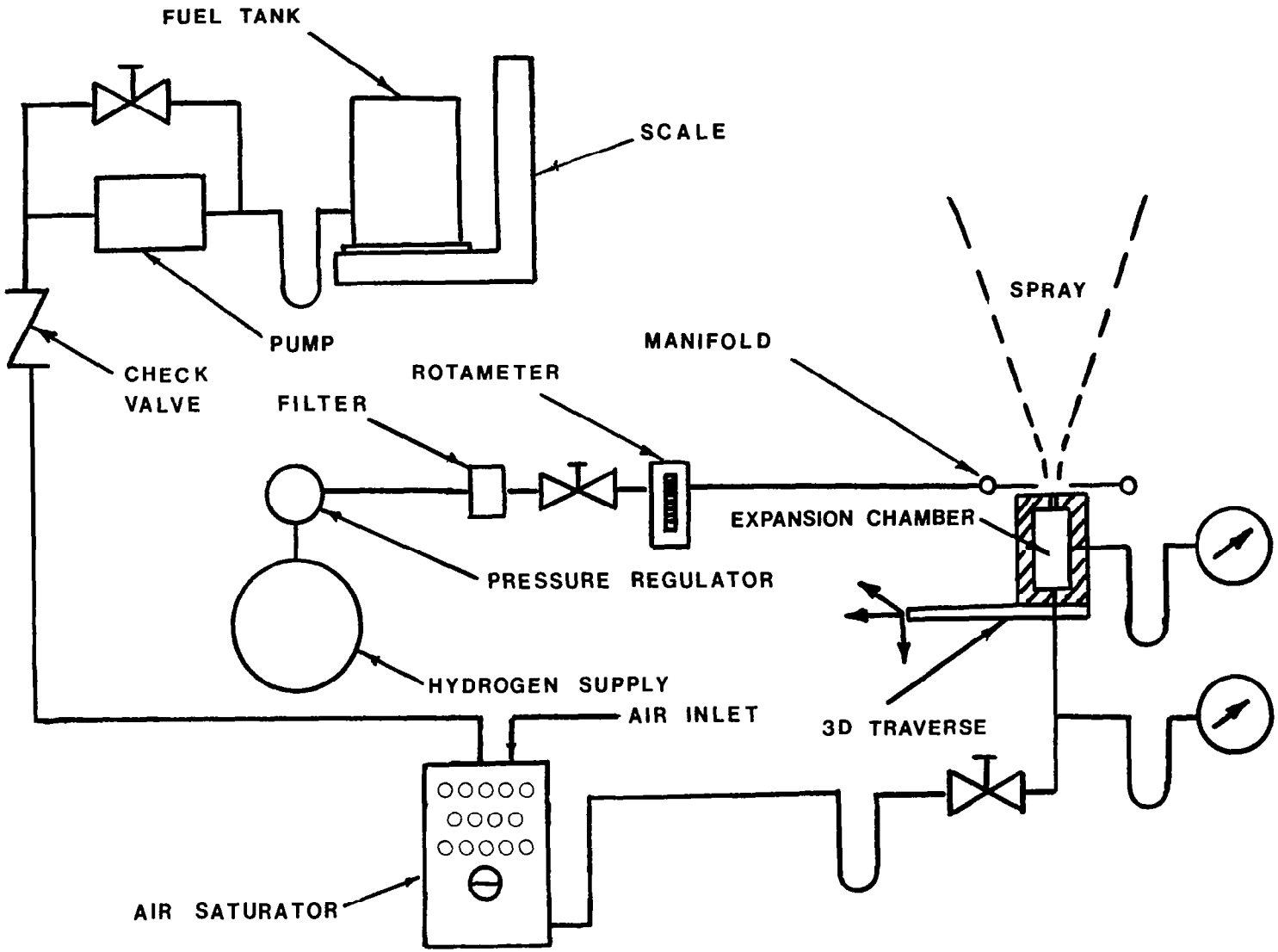

Figure 32. Spray combustion apparatus.

The injector was mounted so that liquid was injected vertically upward. The spray flame was stabilized at the injector exit by an array of four hydrogen-fueled capillary flames. The detailed geometry of the capillary flame configuration is described elsewhere [41].

The fuel storage tank was placed on a scale to allow determination of the mass flow rate by weighing for a timed interval. The fuel was delivered to the aerator by a Whitey, model LD10 Variable Displacement Laboratory Pump. The aerator was a high pressure chamber with its upper portion packed with short sections of glass tubing. This chamber was pressurized with air to the desired saturation pressure. The fuel was delivered to the top of the packing and became saturated with air as it flowed down through the packing. The saturated fuel was collected in a reservoir at the bottom of the aerator where its level could be observed through a sight glass. The fuel then passed from the bottom of the aerator to the injector.

The flow rate of fuel was controlled by selecting the aerator pressure using the pressure regulator on the air supply. The expansion chamber pressure was controlled by adjusting the metering valve at its upstream end. The delivery rate of fuel was manually set to maintain the liquid level in the aerator constant, by adjusting the displacement and bypass flow rate of the pump. The flame was ignited by igniting the four hydrogen capillary flames--initiation of liquid fuel flow then resulted in immediate ignition and stabilization of the spray flame.

The dissolved gas content of the fuel was determined by withdrawing samples and analyzing them in the same manner as Ref. 1. It was found that the present aerator delivered saturated liquid for all operating conditions.

The pressure of the aerator was measured with a Heisse pressure gauge (0.1% accuracy, 0-10.3 MPa range). The expansion chamber pressure was measured with a Validyne No. DP15TL transducer and model CD12 readout unit.

The hydrogen flow to the capillary flames was varied by adjusting the pressure regulator on the outlet of the hydrogen storage cylinder. This flow was metered by means of a critical flow orifice. The saturated air flow rate to the aerator; was metered indirectly from the known flow rate and dissolved air concentration of the fuel.

The flame was photographed using a 4 x 5 Graphlex camera with a 135 mm focal length lens. The camera was mounted on a tripod approximately 3 m from the axis of the flame. All photographs were taken against a black background. Black and white photographs were taken using Type 58 Polaroid film (ASA 400, f-16, 2.5 ms shutter speed). Color photographs were also obtained--using Type 58 Polaroid film (ASA 75, f-10, 2.5 ms shutter speed). Distances on the film were calibrated with two 750W quartz lamps.

3.3 Results and Discussion

Flame photographs were obtained over the same range of operating conditions that were examined during the atomization study. Typical results are illustrated in Fig. 33. Four cases are considered, with an injector inlet pressure of 6.87 MPa; injection without dissolved air for $p_e = p_u$ and $p_e = 0.5\ p_u$; and injection with dissolved air for $p_e = p_u$ and $p_e = 0.5\ p_u$. The last case corresponds to near optimum conditions in the expansion chamber for flashing injection, yielding maximum spray angle and minimum SMD for the injector inlet conditions. The four photographs shown in Fig. 33 were all taken from the same position, with the flame attached at the injector exit (the injector position is only seen clearly on the photograph of combustion with no dissolved gas and $p_e = 0.5\ p_u$, since the bluish flame near the injector in the other cases could not be exposed sufficiently without overexposing the luminous upper portions of the flame).

The results illustrated in Fig. 33 indicate that the presence of dissolved air has little effect on flame shape if the expansion chamber is not used ($p_e = p_u$). In this case, flame widths are roughly the same while flame lengths are slightly longer when dissolved gas is present in comparison to injection of neat liquid. This finding agrees with the results of the atomization study, which showed similar spray angles, but slightly larger SMD when dissolved air was present with no expansion chamber.

When dissolved gas is not present, reduced expansion chamber pressures yield a longer flame, c.f., Fig. 33. In this case, the lower expansion chamber pressure reduces the pressure difference across the injector orifice, yielding poorer atomization, c.f., Fig. 23. Poorer atomization also reduces the spray angle, which is reflected by a reduction of the width of the flame when compared with atomization with no dissolved gas at higher injector pressure ratios.

Finally, operation with optimum expansion chamber conditions and dissolved gas present is seen in Fig. 33 to yield the shortest flame of all the cases shown. Furthermore, the width of the flame near the injector is greatest for this configuration. These effects follow directly from the large spray angles and reduced SMD obtained for optimum flashing injection in comparison to the other cases illustrated in Fig. 33.

The effects observed in Fig. 33 can be primarily attributed to improved atomization rather than effects of premixed combustion due to the presence of dissolved air for the flashing injector tests. In the first place, the concentration of dissolved air is relatively low (roughly 10% on a molar basis) which limits the potential for premixed combustion effects. Secondly, when dissolved gas is present but the expansion chamber is not used, the flame is very similar to that obtained for the injection of neat liquid and, as noted earlier, there is little difference in atomization properties. Test results over the complete

WITHOUT AIR ADDITION

a. Neat liquid $p_e = p_u$.

WITHOUT AIR ADDITION

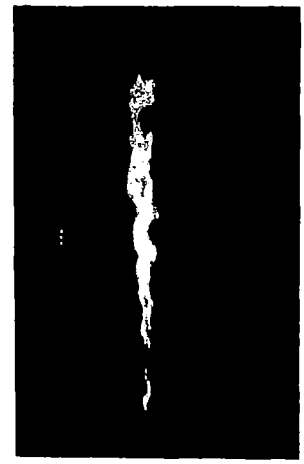

Neat liquid $p_e = 0.5\ p_u$.

WITH AIR ADDITION

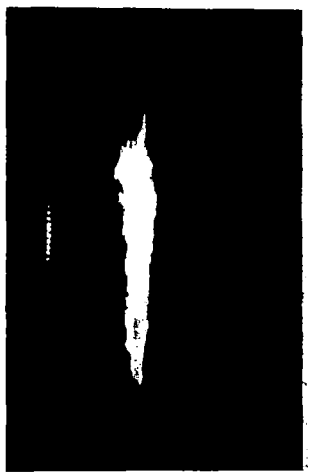

c. Air-saturated liquid, $p_e = p_u$.

WITH AIR ADDITION

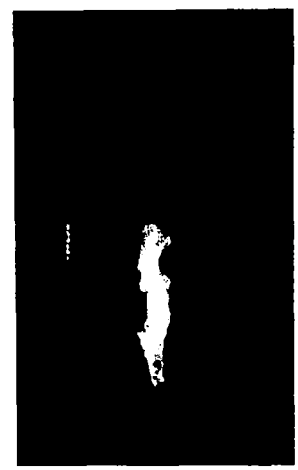

d. Air-saturated liquid, $p_e = 0.5\ p_u$.

Figure 33. Jet A spray flames, $p_u = 6.87$ MPa.

range of variables substantiated this trend--the greatest reduction in flame lengths and the more rapid initial spread of the flame was always associated with conditions that yielded small SMD and large spray angles during the atomization tests.

Since effects of flashing injection on flame shape could generally be attributed to atomization properties, these changes are likely to influence flame radiation, soot production and the generation of pollutants in a conventional manner. In particular, reduced flame lengths should act to reduce the production of soot, due to shorter fuel residence times at fuel-rich high temperature conditions within the core of the flame. Reduced soot concentrations should also have a beneficial effect of reducing flame luminosity and radiation. Quantitative measurements of these effects were not made; however, black smoke was visible at the tip of the longer flames pictured in Fig. 33 while no smoke was observed at the tip of the shorter flame produced under optimum flashing injection conditions.

4. SUMMARY AND CONCLUSIONS

This investigation examined the effect of injecting a flashing liquid on atomization and combustion properties of sprays. The main emphasis of the study was to examine flashing of dissolved air in Jet A fuel; however, flashing of superheated liquids was also considered in order to assist the interpretation of the measurements.

Due to the relatively slow rate of bubble growth in flashing dissolved gas systems, it was found to be necessary to provide an expansion chamber upstream of the injector orifice, in order to obtain appreciable effects of flashing on spray atomization and combustion properties. The effect of this expansion chamber is similar to the gas-liquid mixing section of airblast atomizers; therefore, it was possible to interpret the atomization properties of flashing injectors using results for airblast injectors.

Tests were conducted to determine mass flow rates, drop sizes, spray angles, lqiuid flux distributions and flame shapes for both pure Jet A and Jet A containing dissolved gases. The mass flow rate and spray angle properties of flashing superheated Freon 11 were also investigated. Analysis of mass flow rates and drop sizes was completed in order to assist correlation of the data.

The major conclusions of the study are as follows:

1. An expansion chamber is needed to generate beneficial effects in flashing dissolved gas injection processes due to slow bubble growth rates.
2. For given upstream conditions, an optimum expansion chamber pressure exists where the spray angle is maximized and SMD is minimized. This condition yields the shortest flame lengths, and probably the least soot similar to conventional behavior when atomization is improved for combusting sprays.

3. The present locally homogeneous flow model provided a good estimation of injector flow properties for both flashing liquids containing dissolved gases and superheated liquids. The present separated flow model yielded predictions that were only slightly inferior to the locally homogeneous flow model. Both models indicated that increased spray angles for flashing liquids were generally associated with conditions where the injector orifice was choked and underexpanded.

4. The SMD for the test sprays varied with axial position due to effects of secondary breakup, drop collisions and drop dispersion; therefore, absolute values quoted here are somewhat arbitrary. For measurements made near the location where the SMD was a minimum, the expression due to Mayer [35], Eq. (21), provided the best SMD correlation for injection of pure liquids, while the expression due to Lefebvre [8] for airblast injectors, Eq. (25), provided the best SMD correlation for flashing dissolved gas systems (using the present separated flow model to estimate injector exit conditions). Combining these two expressions provides a means of estimating SMD as a function of expansion chamber pressure for flashing dissolved gas systems.

5. For present test conditions, the expansion chamber generally operated near the boundary of the bubbly and annular flow regimes, cf. Fig. 12. Injector operation yielded a full-cone spray with maximum liquid flux along the centerline for all test conditions.

6. Injector operation was essentially independent of the volume of the expansion chamber for present test conditions. This suggests that the expansion chamber acts similar to the mixing chamber of airblast injectors. Thus, many of the effects observed here for flashing injection with dissolved gases could be obtained in a more conventional manner by using an airblast injector (with somewhat greater design flexibility since air concentrations are not limited by thermodynamic considerations for airblast injectors). Therefore, favorable conditions for application of the flashing injector concept involve cases where the high pressure gas to be dissolved in the fuel is readily available or where a volatile component of the fuel can be easily released by preheating. Good performance in these situations requires the use of an expansion chamber--the results of this investigation should be useful for selecting optimum expansion chamber conditions. A noteworthy feature of the flashing injector concept is that significant modifications of spray angles and SMD could be obtained with relatively low mass qualities of gas - far less gas flow than is normally used for airblast injectors.

REFERENCES

1. S. D. Rupprecht and G. M. Faeth, "An Investigation of Air Solubility in Jet A Fuel at High Pressures," NASA CR 3422, May 1981.

2. C. J. Marek and L. P. Cooper, "Supercritical Fuel Injection System," U. S. Patent No. 4,189,914, February 26, 1980.

3. E. J. Szetela, L. Chiappetta and C. E. Baker, "A Study of External Fuel Vaporization," ASME Paper 81-GT-158, 1981.

4. E. Sher and C. Elata, "Spray Formation from Pressure Cans by Flashing Liquid Jets," AIChE J. 16, 237-242, 1977.

5. R. Brown and J. L. York, "Sprays Formed by Flashing Liquid Jets," AIChE J. 8, 149-153, 1962.

6. M. Suzuki, T. Yamamoto, N. Fatagami and S. Maeda, "Atomization of a Superheated Liquid Jet," Proceedings of First International Conference on Liquid Atomization and Spray Systems, Tokyo, August 1978.

7. K. J. Wu, R. L. Steinberger and F. V. Bracco, "On the Mechanism of Breakup of Highly Superheated Liquid Jets," Paper No. CSS/CI 81-17, The Combustion Institute, Pittsburgh, 1981.

8. A. H. Lefebvre, "Airblast Atomization," Prog. Energy Combust. Sci. 6, 233-261, 1980.

9. W. E. Vensel, "Spray Cap," U. S. Patent No. 2,606,071, August 5, 1952.

10. C. F. Boe, "Triple Expansion Nozzle and Method of Spraying Liquids," U. S. Patent No. 2,585,429, February 12, 1952.

11. F. F. LeGuillou, "Push-Button Having a Calibrated Outlet for a Container Under Pressure," U. S. Patent No. 4,030,667, June 21, 1977.

12. H. K. Forster and N. Zuber, "Growth of a Bubble in a Superheated Liquid," J. Appl. Phys. 25, 474 (1954).

13. J. H. Lienhard, "An Influence of Superheat Upon the Spray Configurations of Superheated Liquid Jets," J. Basic Engr. 88, 685, (1966).

14. J. H. Lienhard, "The Breakup of Superheated Liquid Jets," J. Basic Engr. 92, 515 (1970).

15. J. G. Collier, Convective Boiling and Condensation, 2nd Edition, McGraw-Hill, London (1981).

16. J. H. Rupe, "A Technique for the Investigation of Spray Characteristics of Constant Flow Nozzles," Third Symposium on Combustion and Flame and Explosion Phenomena, pp. 680-694, Williams and Wilkins, Baltimore, 1949.

17. A. J. Shearer and G. M. Faeth, "Evaluation of a Locally Homogeneous Model of Spray Evaporation," NASA CR 3198 (1979).

18. W. F. Ranz, "Principles of Inertial Impaction," Engineering Research Bulletin, B-66, The Pennsylvania State University, 1956.

19. R. A. Dobbins, L. Crocco and I. Glassman, "Measurement of Mean Particle Sizes of Sprays by Diffractively Scattered Light," AIAA J. 1, 1882-1886 (1963).

20. K. R. May, "The Measurement of Airborne Droplets by the Magnesium Oxide Method," J. Scient. Inst. 27, 1950.

21. J. Swithenbank, J. M. Beér, D. S. Taylor, D. Abbot and G. C. McCreath, "A Laser Diagnostic Technique for the Measurement of Droplet and Particle Size Distributions," Experimental Diagnostics in Gas Phase Combustion Systems (B. T. Zinn, Ed.) Progress in Astronautics and Aeronautics, Vol. 53, pp. 421-448, 1977.

22. D. C. Hammond, Jr., "Accuracy Verification of a Malvern ST-1800 Analyzer," Research Publication GMR-3195, General Motors Research Laboratories, 1980.

23. D. C. Hammond, Jr., "Measurements of the Droplet-Size Distributions Produced by the ASTM 'Round-Robin' Nozzle," Research Publication GMR-3668, General Motors Research Laboratories, 1981.

24. C. Harding, "Results of Spray Analysis Performed on the ASTM E-29.04 Round-Robin Water Nozzle using Different Spray Analyzers," Parker-Hannifin Corporation, Technical Information Report DTA 130, 1979.

25. J. M. Tishkoff, "GMR Laser-Video Imaging System Results for the ASTM 'Round-Robin' Nozzle Test," Research Publication GMR-3098, General Motors Research Laboratories, 1979.

26. O. Baker, "Design of Pipe Lines for Simultaneous Flow of Oil and Gas," Oil and Gas J. 26, (1954).

27. J. M. Mandhane, G. A. Gregory and K. Aziz, "A Flow Pattern Map for Gas-Liquid Flow in Horizontal Pipes," Int. J. Multiphase Flow 1, 537-553 (1974).

28. Y. Taitel and A. E. Dukler, "A Model for Predicting Flow Regime Transitions in Horizontal and Near Horizontal Gas-Liquid Flow," AIChE J. 22, 47-55 (1976).

29. G. F. Hewitt and D. N. Roberts, "Studies of Two-Phase Flow Patterns by Simultaneous X-Ray and Flash Photography," AERE-M 2159, HMSO, Great Britain, 1969.

30. T. Oshinowo and M. E. Charles, "Vertical Two-Phase Flow. Part I. Flow Pattern Correlations," Can. J. Chem. Engr. 52, 25-35, (1974).

31. Anon., ASHRAE Handbook and Product Directory, Fundamentals Volume, pp. 16.1-16.4, 1977.

32. D. Chisholm, "Flow of Compressible Two-Phase Mixtures Through Throttling Devices," Chem. and Process Engng., 73-78 (1967).

33. J. W. Daily and D. R. F. Harleman, Fluid Dynamics, Addison-Wesley, Reading, MA, 1966.

34. M. Adelberg, "Mean Drop Size Resulting from the Injection of a Liquid Jet into a High-Speed Gas Stream" AIAA J. 6, 1143-1147 (1968).

35. E. Mayer, "Theory of Liquid Atomization in High Velocity Gas Streams," ARS J. 31, 1783-1785 (1961).

36. R. D. Reitz, "Atomization and Other Breakup Regimes of a Liquid Jet," Ph.D. Thesis, Princeton University, 1978.

37. P. J. O'Rourke and F. V. Bracco, "Modeling of Drop Interations in Thick Sprays and a Comparison with Experiments," Stratified Charge Automotive Engines Conference, The Institution of Mechanical Engineers, London, 1980.

38. G. M. Faeth, "Evaporation and Combustion of Sprays," submitted for publication, 1981.

39. A. J. Shearer, H. Tamura and G. M. Faeth, "Evaluation of a Locally Homogeneous Flow Model of Spray Evaporation," J. of Energy 3, 271 (1979).

40. C-P. Mao, G. A. Szekely, Jr. and G. M. Faeth, "Evaluation of a Locally Homogeneous Flow Model of Spray Combustion," J. of Energy 4, 78 (1980).

41. Ibid., NASA CR 3202, 1980.

APPENDIX A

Table A.1 Mass flow rate data for Jet A saturated with air at 3.45 MPa.

Expansion Chamber Pressure, MPa	Mass Flow Rate, g/s
3.45	1.752
3.34	1.592
2.79	1.415
2.57	1.313
2.31	1.148
1.52	0.895
0.48	0.372

Table A.2 Mass flow rate data for Jet A saturated with air at 6.87 MPa.

Expansion Chamber Pressure, MPa	Mass Flow Rate, g/s
6.87	2.250
6.58	2.180
6.07	2.056
5.79	1.970
5.07	1.820
4.58	1.690
3.10	1.220
1.28	0.558
0.89	0.400

Table A.3 Mass flow rate data for Jet A saturated with air at 10.34 MPa.

Expansion Chamber Pressure, MPa	Mass Flow Rate, g/s
10.34	2.656
10.08	2.604
9.51	2.481
8.58	2.346
7.13	2.049
4.86	1.539
1.65	0.525
1.14	0.458

Table A.4 Mass flow rate data for superheated Freon 11.[a]

Expansion Chamber Pressure, MPa	Mass Flow Rate, g/s
1.73	1.552
1.69	1.399
1.54	1.296
1.35	1.155
1.10	0.979
0.78	0.809
0.34	0.380

[a] p_u = 1.73 MPa, T_u = 370 K

APPENDIX B

Table B.1 Variation of SMD with axial position for injection of Jet A containing no dissolved air at 3.45 MPa.

Axial Distance, cm	SMD, μm
4	65.6
10	63.9
15	55.6
20	48.7
25	47.6
30	45.9
35	46.2
40	49.4
45	51.5

Table B.2 Variation of SMD with axial position for injection of Jet A containing no dissolved air at 6.87 MPa.

Axial Position, cm	SMD, μm
3.2	49.5
6.0	39.2
9.8	32.0
11.4	26.4
11.9	26.5
12.7	27.1
15.2	26.6
18.1	25.2
21.9	26.0
26.0	26.9
29.2	28.1
30.0	29.4
32.0	29.5
34.0	30.9
36.0	32.2
42.0	35.0
46.0	37.5

Table B.3 Variation of SMD with axial position for injection of Jet A containing no dissolved air at 10.34 MPa.

Axial position, cm	SMD, μm
4	40.4
10	19.2
15	18.3
20	19.2
25	20.9
30	22.4
35	24.5
40	26.7
45	27.6

Table B.4 Variation of SMD with axial position for flashing injection of Jet A containing dissolved air.

Axial Position cm	SMD, μm		
	p_u = 3.45 MPa x_u = 0.008 p_e/p_u = 0.44	p_u = 6.87 MPa x_u = 0.017 p_e/p_u = 0.45	p_u = 10.34 MPa x_u = 0.028 p_e/p_u = 0.47
4	62.7	30.1	19.6
10	73.6	29.5	19.4
15	80.1	31.2	22.7
20	80.3	35.4	25.7
25	85.1	41.1	29.2
30	98.1	43.2	31.3
35	106.5	44.6	33.8
40	103.9	48.7	34.4
45	127.8	--	35.5

Table B.5 Variation of SMD with injector orifice inlet pressure for injection of Jet A containing no dissolved air.

Expansion Chamber Pressure, MPa	SMD, μm
p_u = 3.45 MPa	
3.45	60.0
3.35	55.4
3.10	57.1
2.73	60.4
2.42	63.3
2.10	72.2
1.10	134.8
p_u = 6.87 MPa	
6.87	48.5
6.73	46.8
6.60	47.8
5.91	45.8
5.63	46.1
4.95	47.9
4.40	50.0
2.40	63.6
p_u = 10.34 MPa	
10.34	30.4
9.93	29.4
9.62	30.6
9.10	29.5
8.50	31.1
7.70	36.8
6.70	46.7
3.70	

Table B.6 Variation of SMD with expansion chamber pressure for injection of Jet A saturated with air at 3.45 MPa.

Expansion Chamber Pressure, MPa	SMD, μm
3.45	105.9
3.36	91.8
3.20	116.4
2.80	94.5
2.60	79.1
2.30	69.4
1.50	54.3
0.48	82.6

Table B.7 Variation of SMD with expansion chamber pressure for injection of Jet A saturated with air at 6.87 MPa.

Expansion Chamber Pressure, MPa	SMD, μm
6.87	66.34
6.65	62.2
6.40	65.4
6.05	52.8
5.80	51.1
5.05	44.0
4.60	37.5
3.10	27.6
1.40	26.6
0.96	37.4

Table B.8 Variation of SMD with expansion chamber pressure for injection of Jet A saturated with air at 10.34 MPa.

Expansion Chamber Pressure, MPa	SMD, μm
10.34	42.8
9.93	39.4
9.50	34.7
8.90	30.9
8.60	26.0
7.90	23.4
7.14	19.8
4.86	18.2
1.65	22.1
1.14	24.0

APPENDIX C

Table C.1 Variation of spray angle with expansion chamber pressure for injection of Jet A saturated with air at 3.45 MPa.

Expansion Chamber Pressure, MPa	Spray Angle, Deg.
3.45	4.5
3.36	5.0
3.17	5.0
2.79	6.0
2.58	7.3
2.31	8.3
1.53	15.0
0.50	6.3

Table C.2 Variation of spray angle with expansion chamber pressure for injection of Jet A saturated with air at 6.87 MPa.

Expansion Chamber Pressure, MPa	Spray Angle, Deg.
6.87	5.0
6.59	5.0
6.39	5.0
6.05	6.0
5.84	10.0
5.05	15.0
4.57	20.0
3.10	31.0
1.37	20.5
0.96	18.0

Table C.3 Variation of spray angle with expansion chamber pressure for injection of Jet A saturated with air at 10.34 MPa.

Expansion Chamber Pressure, MPa	Spray Angle, Deg.
10.34	5.0
9.93	5.0
9.50	5.0
8.99	6.5
8.58	17.5
7.86	20.5
7.13	28.5
4.81	38.5
1.65	28.3
1.14	22.5

Table C.4 Variation of spray angle with expansion chamber pressure for superheated Freon 11[a]

Expansion Chamber Pressure, MPa	Spray Angle, Deg.
1.73	40.7
1.69	35.7
1.49	42.7
1.27	40.0
0.99	41.0
0.61	48.5
0.18	38.5
0.15	29.0

[a] p_u = 1.73 MPa, T_u = 370 K

1. Report No.	2. Government Accession No.	3. Recipient's Catalog No.
NASA CR-3563		

4. Title and Subtitle	5. Report Date
INVESTIGATION OF SPRAY CHARACTERISTICS FOR FLASHING INJECTION OF FUELS CONTAINING DISSOLVED AIR AND SUPERHEATED FUELS	June 1982
	6. Performing Organization Code
7. Author(s)	8. Performing Organization Report No.
A. S. P. Solomon, L-D. Chen, and G. M. Faeth	None
	10. Work Unit No.
9. Performing Organization Name and Address	11. Contract or Grant No.
The Pennsylvania State University Mechanical Engineering Building University Park, Pennsylvania 16802	NSG-3306
	13. Type of Report and Period Covered
12. Sponsoring Agency Name and Address	Contractor Report
National Aeronautics and Space Administration Washington, D.C. 20546	14. Sponsoring Agency Code 304-00-00

15. Supplementary Notes

Final report. Project Manager, Cecil J. Marek, Aerothermodynamics and Fuels Division, NASA Lewis Research Center, Cleveland, Ohio 44135.

16. Abstract

Flashing injection involves expanding a fluid through an injector until a supersaturated state is reached, causing a portion of the fluid to flash to a vapor. This investigation considered the flow, atomization and spreading properties of flashing injectors flowing liquids containing dissolved gases (Jet/air) as well as superheated liquids (Freon 11). The use of a two-stage expansion process, separated by an expansion chamber, was found to be beneficial for flashing injection--particularly for dissolved gas systems. Both locally homogeneous and separated flow models provided good predictions of injector flow properties. Conventional correlations for drop sizes from pressure atomized and airblast injectors were successfully modified, using the separated flow model to prescribe injector exit conditions, to correlate drop size measurements. Additional experimental results are provided for spray angle and combustion properties of sprays from flashing injectors.

17. Key Words (Suggested by Author(s))	18. Distribution Statement
Fuel injectors Dissolved air Combustor	Unclassified - unlimited STAR Category 07

19. Security Classif. (of this report)	20. Security Classif. (of this page)	21. No. of Pages	22. Price*
Unclassified	Unclassified	89	A05

* For sale by the National Technical Information Service, Springfield, Virginia 22161

NASA-Langley, 1982